First-principles calculation of charge transfer at surfaces: The case of core-excited $Ar^*(2p_{3/2}^{-1}4s)$ on Ru(0001)

Daniel Sánchez-Portal*
Centro de Física de Materiales, Centro Mixto CSIC-UPV/EHU, Apartado 1072, 20080 San Sebastián, Spain and Donostia International Physics Center (DIPC), Paseo Manuel de Lardizabal 4, 20018 San Sebastián, Spain

Dietrich Menzel†
Physik Department E20, Technische Universität München, D-85747 Garching, Germany and Department of Chemical Physics, Fritz-Haber-Institut der Max-Planck-Gesellschaft, Faradayweg 6, 14195 Berlin, Germany

Pedro M. Echenique‡
Centro de Física de Materiales, Centro Mixto CSIC-UPV/EHU, Apartado 1072, 20080 San Sebastián, Spain; Donostia International Physics Center (DIPC), Paseo Manuel de Lardizabal 4, 20018 San Sebastián, Spain; and Departamento de Física de Materiales, Facultad de Química, Universidad del País Vasco (UPV/EHU), Apartado 1072, 20080 San Sebastián, Spain

(Received 5 July 2007; revised manuscript received 17 October 2007; published 5 December 2007)

We present an *ab initio* scheme for the calculation of the resonant charge transfer of electrons at surfaces. The electron initially resides in a bound resonance, i.e., appearing below the vacuum level, associated with a core-excited adsorbate. Our treatment is based on first-principles density-functional calculations of this initial situation using finite slabs. These results are combined with bulk calculations of the substrate material to obtain the Hamiltonian of the semi-infinite system in which the electron evolves. Therefore, we include a realistic description of the electronic structure of both subsystems, substrate and adsorbate, and the interaction between them. The surface Green's function is then computed using the transfer matrix method and projected onto a wave packet localized in the adsorbate. The width and energy of the resonance can be obtained from an analysis of the projected Green's function, and the charge transfer time can be estimated. The calculated width is independent of the wave packet used for the projection, at least as far as there are not several overlapping resonances at neighboring energies. Alternatively, one can directly calculate the time evolution of the population of the initial wave packet. Both alternatives are presented and compared. Our first-principles calculations are based on periodic arrangements of adsorbates on the surface. With an appropriate average of the $\mathbf{k}_\parallel$ resolved results, one can extrapolate to the limit of an isolated adsorbate. We discuss several possibilities to do this. As an application, we focus on the case of the $4s$ bound resonance of a core-excited $Ar^*(2p_{3/2}^{-1}4s)$ adsorbate on Ru(0001), for which there are extensive experimental studies. The calculated values and trends are in good agreement with the experimental observations.

DOI: 10.1103/PhysRevB.76.235406 PACS number(s): 73.20.Hb, 34.70.+e, 73.50.Gr, 71.15.Mb

I. INTRODUCTION

Charge exchange and charge transfer are at the basis of the chemical bond in the ground state. In electronically excited states, charge transfer frequently controls the time of localization of a specific excitation, and therefore the reactivity of such an excited state. Bonding of molecules to surfaces strongly influences their reactivity, both in the ground and in excited states. The experimental finding that the efficiency of electronic excitations to induce reactions is strongly influenced by bonding to a surface[1] can be traced back to the transfer of charge and energy to and from the substrate. It is therefore of paramount importance to get direct access to the time scale of charge transfer at surfaces under well-controlled conditions. The experimental results about the changes of photochemistry of molecules by bonding them to a surface, which have been acquired over decades,[2–5] have clearly shown that these time scales must be very short, i.e., below or around 1 fs or at most some femtoseconds for chemically interesting species. Direct measurements of many processes in surface dynamics, including charge and energy transfer processes, have been done with laser pump-probe techniques;[6–9] they have been very successful in the determination and understanding of surface and image state lifetimes and of energy redistribution processes,[10–12] albeit mostly in the range of tens to hundreds of femtoseconds. The time range of interest for charge transfer in weakly to strongly interacting adsorbate systems—from a few femtoseconds down to a fraction of a femtosecond—is being conquered at present by laser techniques[13] as well, and one can envisage that soon direct results will be available with all the advantages of these methods.

Here, we are concerned with an alternative method which has no difficulties in this time range, although it is somewhat more limited in applicability and measures somewhat different processes. This is the so-called core-hole-clock method which consists in using the lifetime of a certain core hole of an atom—which, in many cases, is in the low femtosecond range—as a time standard. Recording the decay spectra of a resonantly excited core-hole state of an atom bound to a surface leads to two separable sets of spectra: one of them

corresponds to decay before and the other after the initially excited electron has been transferred into the substrate. The ratio of the integrals of these peaks, i.e., the branching ratio of these two competing processes, gives the ratio between the time scales of the charge transfer and the core-hole decay processes.[14–16] Since the core-hole decay time is usually quite well known, the charge transfer time can be extracted. This approach is particularly powerful when used with narrow-band excitation, i.e., with bandwidths of the exciting radiation which are below the lifetime width of the core hole, the so-called Auger-resonant Raman conditions.[17] The method measures the charge transfer of an excited electron localized on a single atom with a core hole, which can even be selected in the presence of other atoms of the same kind (e.g., first monolayer species against second or higher monolayers). The core hole and the strong localization of the initial state on an atom conceivably may lead to differences compared to laser results concerned with extended orbitals (see also below). Using this method, even the variation of the charge transfer time with varied excitation energy, i.e., with the different number and character of available electronic final states in the substrate as a function of the energy, can be measured. A number of well-defined systems have been studied in the past years.[14,15,18–20] Since the branching ratio described can usually be recorded confidently from 10:1 to 1:10 (with ratio 1:1 corresponding to core-hole decay and charge transfer having the same time constant), the accessible processes are determined by the absolute value of the core-hole lifetime. Thus, by using very fast Coster-Kronig decay processes, it has been possible recently to push the measured charge transfer time into the attosecond range as necessary for a strongly chemisorbed species.[21]

In particular, a systematic set of data has been measured for adsorbed argon atoms on various substrates and with varying coupling strengths using layers of argon and xenon as spacers.[20,22] Adsorbed Ar atoms are a particularly well suited system because their $p^{3/2}$ level (at about 245 eV) lies in a very well suited energy range and its strong and well separable two sets of decay spectra (we emphasize that, as the initial state of decay is the core-excited Ar atom—see the treatment below—a proper comparison with, e.g., laser measurements would be adsorbed K, the core-equivalent atom). One intriguing aspect of the data was that in several cases, the charge transfer time increased when the energy of the photons used for the initial excitation was increased. In a simplified model, this corresponds to shifting the position of the excited level to higher energies, i.e., closer to the vacuum level.[18,20,22] This is contrary to expectation from a simple tunneling picture as for it the tunneling rate should exponentially increase with decreasing barrier height. Therefore, it became clear that the band structure of the substrate receiving the charge is of importance. Theoretical modeling of the latter as well as of the entire process should then lead to improved understanding of the charge transfer process. Since the most complete set of data had been accumulated for Ar on the close-packed Ru(0001) surface,[18,20] we have decided to try to tackle this system. In what follows, we describe a calculation of the charge transfer time from a bound 4*s* resonance in an adsorbed core-ionized Ar on Ru(0001) using first-principles methods.

In order to present the details of our calculational method, let us start by considering the time evolution of an electron which has been promoted to a well-defined excited state Ψ_R, with energy ϵ_R, of a certain "small" system adsorbed on a metallic substrate. Small here means that the system is described by a Hamiltonian $\hat{H}_A$ with a discrete spectrum of bound states, such as an atom or a small molecule. On the other hand, the substrate exhibits a continuum spectrum, described by some effective Hamiltonian $\hat{H}_S$. In the presence of a substrate-adatom interaction $\hat{V}$, there is a finite probability that the electron will be transferred into the substrate after a certain time. Ψ_R becomes then what is usually called a resonance. It does not have any longer a well-defined energy, since it is not an eigenstate of the combined substrate-adsorbate system $\hat{H}_{AS}=\hat{H}_A+\hat{H}_S+\hat{V}$, but its spectral weight spreads over an energy region of width η, which is inversely proportional to the typical charge transfer time.

The time evolution of the electron can be efficiently characterized by the so-called survival amplitude[23]

$$A(t) = \langle \Psi_R | \Psi(t) \rangle, \tag{1}$$

with $|\Psi_R\rangle = |\Psi(t=0)\rangle$. The probability to find the electron in the initial state ($|\Psi_R\rangle$) after some time t is then given by $|A(t)|^2$. $A(t)$ can be easily expressed in terms of the eigenstates Φ_n and energies E_n of the combined Hamiltonian $\hat{H}_{AS}$,

$$A(t) = \sum_n |\langle \Psi_R | \Phi_n \rangle|^2 e^{-iE_n t}. \tag{2}$$

The Fourier transform of $A(t)$ is proportional to the projection of the Green's function on the initial state,

$$\tilde{A}(\omega) = \frac{1}{\pi} \lim_{\delta \to 0^+} \sum_n \int_0^\infty dt |\langle \Psi_R | \Phi_n \rangle|^2 e^{-[i(E_n-\omega)+\delta]t}$$

$$= \frac{i}{\pi} \langle \Psi_R | \hat{G}(\omega) | \Psi_R \rangle = \frac{i}{\pi} G_{RR}(\omega). \tag{3}$$

It is quite simple to show that $G_{RR}(\omega)$ can be written as[24] $[\epsilon_R - \omega - f(\omega) + i\eta(\omega)]^{-1}$, where

$$f(\omega) = P \int_{\epsilon_{min}}^{\epsilon_{max}} d\epsilon \frac{|V(\epsilon)|^2 \rho(\epsilon)}{\epsilon - \omega},$$

$$\eta(\omega) = \pi |V(\omega)|^2 \rho(\omega). \tag{4}$$

Here, $V(\epsilon)$ is the interaction between the adsorbate and a given state of the substrate with energy ϵ, and $\rho(\epsilon)$ the substrate density of states. In deducing Eq. (4), we have assumed orthogonality between the resonance and the states of the substrate and that the sole dependence of the interaction is on the energy of the final state. The latter assumption is, however, unnecessary, and the index ϵ can be replaced by a collection of appropriate quantum numbers. It is usually assumed that the main effect of the interaction with the substrate is just a small shift in the energy position of the resonance and to provide a finite width, $\eta = \pi |V(\epsilon_R)|^2 \rho(\epsilon_R)$. In this case, the decay of the resonance population is purely exponential $|A(t)|^2 = e^{-\pi t}$, with a characteristic lifetime τ

$=\frac{1}{2}\eta^{-1}$. However, even when $\hat{V}$ is a small perturbation, the behavior can be more complicated depending on the details of the substrate electronic structure. For example, if $\hat{V}$ is roughly energy independent and the resonance is coupled to a two-dimensional continuum [i.e., $\rho(\epsilon)$ is a constant] such as, for example, a surface state with parabolic dispersion, then it can be shown[23] that an additional resonance (peak) ϵ_R' always appears below the continuum. This is due to the logarithmic divergence of $f(\omega)$ when ω approaches the bottom of the band ($\omega \to \epsilon_{min}^-$), which guarantees that $\epsilon_R' = \epsilon_R + f(\epsilon_R')$ has always a solution with $\epsilon_R' < \epsilon_{min}$. The consequences of this and related effects have been recently observed for the Cu(111) and Ag(111) surfaces: The surface state localizes around the adatoms, and a clear spectroscopic signal appears in their neighborhood below the surface band minimum.[25,26]

In this paper, we aim at a realistic calculation of the resonant transfer of an electron initially residing in an excited state of an atom adsorbed on a metallic substrate. The purpose is to include in our description (i) all the details of the electronic structure of the substrate and (ii) an accurate description of the strength and final-state dependence of the substrate-adsorbate interaction. We therefore use density-functional calculations of the combined adsorbate-substrate system to provide the necessary input for the computation of Eq. (3). We apply this methodology to the case of an adlayer of Ar deposited on Ru(0001). This system has been very well characterized, and there exist high-resolution measurements of the charge transfer rates using resonant Auger spectroscopy.[18,20] In these experiments, an electron is initially promoted from the $2p$ inner shell of one of the Ar atoms into a bound resonance originated from the $4s$ atomic state of the same atom. The core-hole decay then proceeds via an Auger process. As explained in detail in Ref. 20, the Auger decay can take place before or after the initially excited electron has been transferred to the substrate, giving rise to two different signatures in the spectra. The final state, after the Auger decay, is, in both cases, a doubly ionized argon atom in the overlayer. The initial state is an isolated core-excited "impurity" $\mathrm{Ar}^{\star}(2p_{3/2}^{-1}4s^{+1})$ in the Ar overlayer. Due to the interaction with the core hole, the $4s$ state of the $\mathrm{Ar}^{\star}$ atom forms an impurity level located well within the energy gap of the Ar layer. This has at least two implications: (i) the $4s$ impurity level is well localized on the core-excited atom and (ii) for a freestanding Ar layer, this level has a well-defined energy ϵ_{4s} and wave function Ψ_{4s}. Point (i) will facilitate the development of an approximate scheme to perform self-consistent density-functional calculations of this initial situation as described in detail below. Based on point (ii), we will identify Ψ_{4s} with the resonance wave packet Ψ_R introduced in the previous paragraph. However, it is important to stress that the our final results for the resonance width and energy are independent of this choice, at least as far as the wavepacket used to project the Green's function Ψ_R has a large overlap with the true wave function of the resonance as it is the case here.

II. THEORETICAL BACKGROUND

A. Green's function of the semi-infinite system

In the previous section, we have seen that the dynamics of a given electronic state can be easily expressed in terms of the one-electron Green's function. We want to make our description as accurate as possible and, therefore, use first-principles methods for this calculation. Unfortunately, most of the standard methods to perform first-principles calculations of surfaces rely on the use of relatively thin slabs. This approximation is justified by the assumption that most surface properties converge rapidly with the number of atomic layers in the slab. Typical examples are, for many systems, the atomic structure and relaxations of the surface layer, the adsorption energies of small adsorbates, the electronic density in the surface region, etc. Other properties, particularly those dependent on the precise energetic position of the electronic levels, converge quite slowly and even show oscillations as a function of the number of layers in the slab. This is related to the confinement of the electronic states in the direction perpendicular to the slab surfaces, causing the discretization of the spectrum. For this reason, it is quite difficult to directly use the electronic eigenfunctions and eigenvalues obtained from the slab to calculate accurately the Green's function in Eq. (3). The typical differences between the energy positions of the subbands in the slab [$\delta E \sim (\pi/L)^2$, with L the thickness of the slab] are larger than or comparable to the peak widths that we want to resolve in our calculation ($\leqslant$600 meV corresponding to charge transfer times $\geqslant$1 fs). In other words, the energy resolution provided by a slab calculation is insufficient for our purposes. Niedfeldt *et al.*[27,28] have recently developed a deconvolution scheme to try to extract the width of the adsorbate energy levels from the discrete spectrum obtained using density-functional slab calculations and applied it to Li on different metallic substrates. Here, we have decided to adopt a different approach: to calculate the Green's function of a truly semi-infinite system, thus avoiding finite size effects.

Several methodologies have been designed over the years to try to overcome the limitations of the slab models for surface calculations. The most powerful is probably the so-called embedding method developed by Inglesfield.[29–33] The embedding and other similar methods are designed to perform self-consistent calculations in systems where the bulk periodicity is broken by defects, impurities, surfaces, or interfaces. In practice, however, their implementations can be cumbersome and, in many cases, they are restricted to deal with particular geometries that allow performing necessary simplifications. This has probably prevented their wider application to date.

The method that we describe here is certainly related to many of these schemes, although somewhat simpler. Our idea is to combine standard density-functional calculations using finite slabs with the use of recursive methods to obtain the Green's function of the surface. The main hypothesis is that we can use thick enough slabs to obtain a reasonably good description of the electronic density and potential at the surface. We thus obtain the electronic Hamiltonian of the surface region from density-functional calculations using finite slabs. This information (Hamiltonian matrix elements) is later combined with that obtained from a bulk calculation of the substrate material. The use of a basis set localized in real space is instrumental for this purpose. We thus use a linear combination of numerical atomic orbitals as a basis set for our *ab initio* calculations.[34,35] The Hamiltonian automatically

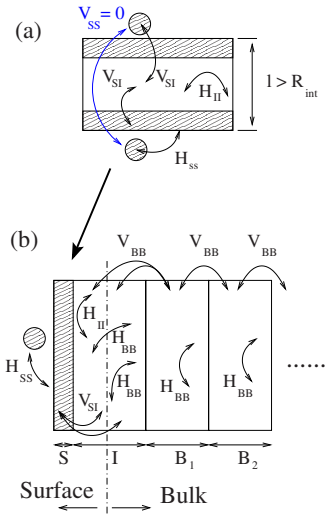

FIG. 1. (Color online) (a) We typically use symmetric slabs in our *ab initio* calculations. Surface regions (dashed areas) are defined in such a way that the matrix elements of the Hamiltonian between them are strictly zero or negligible. This requires the thickness of the slab L to be larger that the interaction range R_{int}. (b) Schematic representation of the partition of the semi-infinite system in regions having only nearest-neighbor interactions. The system is divided into a surface region (S), an intermediate region (I), and an infinite number of identical bulk regions (B_i, $i=1,\ldots,\infty$). The interactions within the S region (H_{SS}), some of the interactions in the I region (H_{II}), and the interactions between the S and I regions (V_{SI}) are obtained from a slab calculation as indicated in (a). The H_{BB} and V_{BB} interactions are obtained from a bulk calculation.

assumes a tight-binding-like form. The matrix elements of the Hamiltonian and overlap between atoms that are far apart (beyond $R_{int}\sim 15$ Å for the system studied here) are strictly zero, and the infinite system can be divided into groups of atomic layers ("regions") that only interact with the nearest-neighbor groups [see Fig. 1(b)]. The Hamiltonian (and overlap) matrix elements within the surface region (S) are obtained from the slab, while those of the inner regions (bulk regions, B_i) are taken from a bulk calculation using similar parameters. A common energy reference is set by aligning the Fermi levels of both calculations (this is possible since we are dealing with metals here; for insulators or semiconductors, the average potential should be aligned instead). An intermediate region (I) is also defined, where the "character" of the interactions changes from slablike to bulklike. In particular, the interactions between the I and S regions and those of the atoms in I closer to the surface are taken from the slab calculation. The interaction between the I and B_1 regions and those of the atoms in I closer to the bulk come from a bulk calculation. We refer to Fig. 1 and its caption for a detailed explanation of this partition scheme.

We can now use the recursive relation

$$\sum_j G^{ij}(\omega,\mathbf{k}_\parallel)[H_{jk}(\mathbf{k}_\parallel)-\omega S_{jk}(\mathbf{k}_\parallel)]=\delta_k^i \tag{5}$$

to obtain the Green's function in the surface region for each crystalline momentum parallel to the surface plane, $\mathbf{k}_\parallel$. We always use supercells in the lateral directions; $\mathbf{k}_\parallel$ is a well-defined quantum number in our calculations, therefore. We use the notation proposed by Artacho and Miláns del Bosch[36] for nonorthogonal basis sets. Lower indices correspond to matrix elements calculated using the original basis orbitals, while upper indices refer to matrix elements calculated using the dual basis set. The matrix elements of the Green's function are defined here such that

$$G(\mathbf{r},\mathbf{r}';\omega,\mathbf{k}_\parallel)=\sum_{ij} G^{ij}(\omega,\mathbf{k}_\parallel)\phi_i(\mathbf{k}_\parallel,\mathbf{r})\phi_j^\star(\mathbf{k}_\parallel,\mathbf{r}'), \tag{6}$$

where $\phi_i(\mathbf{k}_\parallel,\mathbf{r})$ are the basis functions, Bloch-like combinations of the atomic orbitals $\varphi_i(\mathbf{r})$ at the atomic positions $\mathbf{R}_\alpha$,

$$\phi_i(\mathbf{k}_\parallel,\mathbf{r})=\sum_\alpha e^{-i\mathbf{k}_\parallel\cdot\mathbf{R}_\alpha}\varphi_i(\mathbf{r}-\mathbf{R}_\alpha). \tag{7}$$

$H_{jk}(\mathbf{k}_\parallel)$ and $S_{jk}(\mathbf{k}_\parallel)$ are, respectively, the matrix elements of the Hamiltonian and the overlap matrix in such a basis set. Using the partition of the system given in Fig. 1, we can rewrite Eq. (5) as (for simplicity, we drop the $\mathbf{k}_\parallel$ index for the time being; we will reintroduce it later in this section)

$$G^{SS}(\omega)M_{SS}(\omega)+G^{SI}(\omega)M_{IS}(\omega)=\delta_S^S,$$

$$G^{SS}(\omega)M_{SI}(\omega)+G^{SI}(\omega)M_{II}(\omega)+G^{SB_1}(\omega)M_{B_1I}(\omega)=0,$$

$$G^{SI}(\omega)M_{IB_1}(\omega)+G^{SB_1}(\omega)M_{B_1B_1}(\omega)+G^{SB_2}(\omega)M_{B_2B_1}(\omega)=0,$$

$$G^{SB_{(n-1)}}(\omega)M_{B_{(n-1)}B_n}(\omega)+G^{SB_n}(\omega)M_{B_nB_n}(\omega)+G^{SB_{(n+1)}}(\omega)M_{B_{(n+1)}B_n}(\omega)=0, \tag{8}$$

where $M_{xy}(\omega)=H_{xy}-\omega S_{xy}$. The last equation in Eq. (8) can be solved using the transfer matrix scheme,[37–42] where we write $G^{SB_{(n+1)}}(\omega)=G^{SB_n}(\omega)T(\omega)$ with T the so-called transfer matrix. The resulting equation is independent of the index n and can be solved by iteration:[38]

$$T(\omega)=(\omega S_{BB'}-V_{BB'})[(H_{BB}-\omega S_{BB})+T(\omega)(V_{BB'}^\dagger-\omega S_{BB'}^\dagger)]^{-1}. \tag{9}$$

H_{BB} and $V_{BB'}$ are, respectively, the interactions *within* and *between* the neighboring bulk regions, as defined in Fig. 1 (S_{BB} are $S_{BB'}$ are the corresponding overlaps). In order to converge this iteration, it is necessary to evaluate the Green's function outside the real axis. For this, we need to add a small imaginary part to the energy $\omega+i\delta$. Once $T(\omega)$ is known, all the equations in Eq. (8) can be solved and $G^{SS}(\omega)$ obtained. Finally, the initial electronic wave packet is expressed in terms of the Bloch combinations of numerical atomic orbitals in the surface region,

$$\Psi_R(\mathbf{k}_\parallel,\mathbf{r})=\sum_i c_R^i(\mathbf{k}_\parallel)\phi_i(\mathbf{k}_\parallel,\mathbf{r}), \tag{10}$$

and the projection of the Green's function onto this state gives

$$G_{RR}(\omega,\mathbf{k}_\parallel)=\sum_{ijkl} c_R^{i\star}(\mathbf{k}_\parallel)S_{ik}(\mathbf{k}_\parallel)G^{kl}(\omega,\mathbf{k}_\parallel)S_{lj}(\mathbf{k}_\parallel)c_R^{j}(\mathbf{k}_\parallel), \tag{11}$$

where $S_{ij}(\mathbf{k}_\parallel)$ is the overlap corresponding to orbitals i and j. We have recently used a similar approach to compute the width of the quantum well states of Cs and Na overlayers on Cu(111), obtaining results in good agreement with the experiment.[43]

B. Charge transfer time

Equation (3) provides the relation between the projected Green's function and the time evolution of the initial wave packet $\Psi_R(\mathbf{k}_\parallel,\mathbf{r})$. We now fit, in an energy range of ±4 eV around the position of the maximum, $G_{RR}(\omega,\mathbf{k}_\parallel)$ with an expression of the form

$$G_{RR}(\omega,\mathbf{k}_\parallel)\approx\sum_i \frac{A_i}{(\omega-\epsilon_i)+i\Gamma_i/2}. \tag{12}$$

We typically need between one and three (sometimes more) different values of A_i, ϵ_i, and Γ_i, depending on $\mathbf{k}_\parallel$, to have a reasonable fit of the Green's function in the selected energy range. This is due to the presence of surface states and resonances associated with the ruthenium in addition to the Ar* resonance that we want to study here. However, it is always possible to make a clear identification of one of these peaks with the 4s resonance associated with the Ar* atoms in the surface. In fact, the energy position of the Ar* resonance can be usually anticipated from the slab calculation by inspecting the band structure and analyzing the Mulliken populations[44] of the different eigenstates of the slab. Thus, we obtain the energy position $\epsilon_R(\mathbf{k}_\parallel)$ and width $\Gamma_{fit}(\mathbf{k}_\parallel)$ of the resonance as a function of $\mathbf{k}_\parallel$. Indeed, to obtain the physical width of the level, we have to subtract the small imaginary part added to the frequency in the calculation of the Green's function (see Sec. II A), $\Gamma_R(\mathbf{k}_\parallel)=\Gamma_{fit}(\mathbf{k}_\parallel)-2\delta$. In the calculation presented here, we have used $\delta=100$ meV. The use of this relatively large value is very convenient since it decreases the computational time considerably. We have checked that using smaller values (30 and 10 meV), we get very similar results for $\Gamma_R(\mathbf{k}_\parallel)$.

The population of the wave packet $\Psi_R(\mathbf{k}_\parallel,\mathbf{r})$ can now be assumed to decay exponentially with a time constant (charge transfer time) $\tau_{CT}(\mathbf{k}_\parallel)=\Gamma_R(\mathbf{k}_\parallel)^{-1}$. We keep the $\mathbf{k}_\parallel$ index explicitly to stress that all our calculations are performed for periodic supercells along the surface. Therefore, we do not have an isolated Ar* on the surface, but a periodic array of them. This will be explained in more detail below when we will describe the systems for which we have performed the actual calculations. The real experimental situation corresponds to a very small concentration of excited atoms at a given time, i.e., we should consider isolated photoexcited atoms in the argon layer. We can use our data, corresponding to periodic arrays, to estimate the charge transfer time from an isolated excited atom. For this purpose, we need to perform a proper average of $\Gamma_R(\mathbf{k}_\parallel)$ over the whole surface Brillouin zone of our supercells. We can do this easily using Wannier-like transformations. A well-defined band can always be described in terms of Bloch-like delocalized wave functions or alternatively localized wave packets $W_R(\mathbf{r})$:

$$\Psi_R(\mathbf{k}_\parallel,\mathbf{r})=\sum_\alpha e^{-i\mathbf{k}_\parallel\cdot\mathbf{R}_\alpha}W_R(\mathbf{r}-\mathbf{R}_\alpha),$$

$$W_R(\mathbf{r})=\frac{1}{N_{\mathbf{k}_\parallel}}\sum_{\mathbf{k}_\parallel}\Psi_R(\mathbf{k}_\parallel,\mathbf{r}). \tag{13}$$

Here, $N_{\mathbf{k}_\parallel}$ is the number of k points in the supercell Brillouin zone, and the sum in α runs over a similar number of neighbors consistently with the Born–von Karman boundary conditions.[45] We now calculate the survival probability amplitude of the localized wave packet,

$$\begin{aligned}A_W(t)&=\langle W_R(t=0)|W_R(t)\rangle\\&=\frac{1}{N_{\mathbf{k}_\parallel}^2}\sum_{\mathbf{k}_\parallel}\langle\Psi_R(\mathbf{k}_\parallel,t=0)|\Psi_R(\mathbf{k}_\parallel,t)\rangle\\&\approx\frac{1}{N_{\mathbf{k}_\parallel}^2}\sum_{\mathbf{k}_\parallel}\langle\Psi_R(\mathbf{k}_\parallel)|\Psi_R(\mathbf{k}_\parallel)\rangle e^{-i\epsilon_R(\mathbf{k}_\parallel)t}e^{-\Gamma(\mathbf{k}_\parallel)t/2}.\end{aligned} \tag{14}$$

$A_W(t)$ reflects two different electron dynamics. The decay into the substrate states is represented by the real exponentials. We also have a term related to the $\mathbf{k}_\parallel$ dependence of the energy of the resonance. This term describes an artificial dynamics associated with the spurious dispersion of the resonance band, i.e., with the hopping of the excited electron between neighboring Ar* atoms. For an isolated impurity, the dispersion of the band should be zero, i.e., $\epsilon_R(\mathbf{k}_\parallel)$ should be independent of $\mathbf{k}_\parallel$. We, thus, can substitute this by an appropriate average $\bar{\epsilon}_R$. We define the survival amplitude for the *isolated* wave packet as

$$\begin{aligned}A_{isol}(t)&=\frac{e^{-i\bar{\epsilon}_R t}}{N_{\mathbf{k}_\parallel}^2}\sum_{\mathbf{k}_\parallel}\langle\Psi_R(\mathbf{k}_\parallel)|\Psi_R(\mathbf{k}_\parallel)\rangle e^{-\Gamma(\mathbf{k}_\parallel)t/2}\\&=\frac{e^{-i\bar{\epsilon}_R t}}{N_{\mathbf{k}_\parallel}}\sum_{\mathbf{k}_\parallel}S_{WW}(\mathbf{k}_\parallel)e^{-\Gamma(\mathbf{k}_\parallel)t/2},\end{aligned} \tag{15}$$

where

$$S_{WW}(\mathbf{k}_\parallel)=\sum_\alpha e^{-i\mathbf{k}_\parallel\cdot\mathbf{R}_\alpha}\langle W_R(\mathbf{r})|W_R(\mathbf{r}-\mathbf{R}_\alpha)\rangle. \tag{16}$$

From here, we can easily define an effective decay rate for $|A_{isol}(t)|^2$. To first order in t, we have

$$|A_{isol}(t)|^2\approx 1-\frac{1}{N_{\mathbf{k}_\parallel}}\sum_{\mathbf{k}_\parallel}S_{WW}(\mathbf{k}_\parallel)\Gamma(\mathbf{k}_\parallel)t, \tag{17}$$

and, thus, we can define

$$\Gamma_{isol}=\frac{1}{N_{\mathbf{k}_\parallel}}\sum_{\mathbf{k}_\parallel}S_{WW}(\mathbf{k}_\parallel)\Gamma(\mathbf{k}_\parallel). \tag{18}$$

Notice that

$$\frac{1}{N_{\mathbf{k}_\parallel}}\sum_{\mathbf{k}_\parallel} S_{WW}(\mathbf{k}_\parallel) = 1 \tag{19}$$

if $W_R(\mathbf{r})$ is normalized. The values of $\Gamma(\mathbf{k}_\parallel)$ are directly obtained from our first-principles calculations. They carry all the information about the electronic structure of the substrate and the coupling between the Ar* resonance and the states of the metal. For example, $\Gamma(\mathbf{k}_\parallel)$ is zero for regions of the supercell Brillouin zone where we have projected band gaps of the substrate (i.e., no states of the metal substrate available for decay). It also becomes quite small for regions with a depleted density of states in the metal. However, we do not have direct access to the wave function of the "localized" resonance. For reasonably large supercells, this is not a serious limitation since the overlap between localized wave packets $W_R(\mathbf{r})$ in neighboring supercells is very small and $S_{WW}(\mathbf{k}_\parallel)\approx 1$. In our case, we have an approximate $S_{WW}(\mathbf{k}_\parallel)$ by the overlap, constructed using $4s$ orbitals of the excited Ar atoms $S_{4s^\star,4s^\star}(k_\parallel)$ in our periodic slab. In fact, for the 3×3 and 4×4 supercells (see below), this overlap is always equal to 1 and independent of $\mathbf{k}_\parallel$, indicating that there is no appreciable overlap between the $4s$ orbitals of Ar* atoms in neighboring supercells. However, for the smaller 2×2 supercell, the term $S_{4s^\star,4s^\star}(k_\parallel)$ provides a different weight for different regions of the supercell Brillouin zone: It increases the relative importance of the region near the origin (Γ point) for the final value of Γ_{isol}.

In Eq. (18), we first find the width of the resonance $\Gamma(\mathbf{k}_\parallel)$ as a function of $\mathbf{k}_\parallel$ and then we average it over the supercell Brillouin zone. Alternatively, we could follow our reasoning in Eq. (15) and obtain an expression for $A_{isol}(t)$ in terms of our calculated Green's functions:

$$A_{isol}(t) = e^{-i\bar{\epsilon}_R t}\int_{-\infty}^{\infty} d\omega e^{-i\omega t}\tilde{A}_{isol}(\omega), \tag{20}$$

where

$$\tilde{A}_{isol}(\omega) = \frac{i}{\pi N_{\mathbf{k}_\parallel}}\sum_{\mathbf{k}_\parallel} S_{WW}(\mathbf{k}_\parallel) G_{RR}(\omega - \epsilon_R(\mathbf{k}_\parallel), \mathbf{k}_\parallel). \tag{21}$$

Therefore, we first analyze the Green's function calculated for each k point to obtain $\epsilon_R(\mathbf{k}_\parallel)$ (i.e., the position of the main peak as a function $\mathbf{k}_\parallel$). We use these values to fix the zero of energy (frequency) of the Green's function as a function of $\mathbf{k}_\parallel$ and to perform the average in Eq. (21). Γ_{isol} can now be obtained from a fit of $\mathrm{Re}[\tilde{A}_{isol}(\omega)]$ to a Lorentzian profile. Both methods, the one based on Eq. (18) and that based on Eq. (21), provide quite similar results. This can be appreciated in data shown in Table I that will be commented on below in more detail.

Once Γ_{isol} has been calculated, we define the charge transfer time for the isolated excited atom as $\tau_{CT}=1/\Gamma_{isol}$.

C. Time evolution of the population of an initial wave packet

In the previous sections, we have described a method to calculate the surface Green's function with high energy resolution. This Green's function can be projected onto a wave packet with a large overlap with the wave function of the resonance that we want to study. Then, the width and energy of the resonance can be extracted from an analysis of this projected Green's function. The calculated results are, to a high degree, independent of the wave packet used for the projection.

TABLE I. Estimated widths of the $4s$ Ar* resonance as a function of the distance between an adlayer lattice parameter $d_{\text{Ar-Ar}}=2.702$ Å and the metallic surface $d_{\text{Ru-Ar}}$. As described in the text, we have used two possible ways to analyze the Green's function calculated using a 3×3 lateral supercell and Ar layer.

	$\Gamma_{isol}^{\mathrm{Ar}^*\,4s}$ (meV) 3×3 supercell	
$d_{\text{Ru-Ar}}$ (Å)	Method 1 [Eq. (27)]	Method 2 [Eq. (21)]
6.0	160	150
5.0	194	174
4.0	176	156
3.5	272	264
3.14	472	554

Alternatively, one can explicitly calculate the time evolution of the population of a given wave packet initially localized in the surface region. In this case, the results will depend on the selected wave packet. In particular, the wave packet may contain significant contributions from several resonances and/or the continuum, and its time evolution can significantly deviate from a simple exponential decay. However, in some cases, this calculation may be a better representation of some real experimental situations, for example, when the initial excitation is produced by light pulses of very short duration (i.e., with very limited energy resolution). One should stress here that this is not the case for the core-hole-clock spectroscopy experiments, which are typically performed with highly monochromatic light.[20]

We will use Eqs. (20) and (21) to calculate the dynamics of the initial wave packet. However, in order to obtain physical results, one should take into account the energy of final states in the substrate. The states below the Fermi energy (E_F) are occupied and should not be available for the propagation of our excited electron. To enforce this restriction, we introduce an energy cutoff into the function $\tilde{A}_{isol}(\omega)$ calculated in Eq. (21). We thus have

$$\mathrm{Re}[\tilde{A}_{isol}^{cut}(\omega)] = \mathrm{Re}[\tilde{A}_{isol}(\omega)][1-f(\omega)], \tag{22}$$

where f is the Fermi-Dirac distribution $f(\omega)=(1+e^{\beta(\omega-E_F)})^{-1}$. Although physically well motivated, this abrupt energy cutoff can, at least in principle, introduce spurious oscillations in the time propagation. This is not the case in practice: The calculated time evolution is quite independent of the value given to β (we have varied β^{-1} in the range from 25 meV to 1 eV obtaining always very similar results). This reflects that, in accordance with the experimental situation that we want to study, our initial wave packet corresponds to a resonance centered at energies well above E_F. Already in $G_{RR}(\omega,\mathbf{k}_\parallel)$, most of the spectral weight corresponds to ener-

gies above E_F. We can obtain the imaginary part of $\tilde{A}^{cut}_{isol}(\omega)$ using the relation

$$\mathrm{Im}[\tilde{A}^{cut}_{isol}(\omega)] = P\int_{-\infty}^{\infty} d\omega' \frac{\mathrm{Re}[\tilde{A}^{cut}_{isol}(\omega')]}{\omega - \omega'}. \quad (23)$$

We finally calculate the time evolution of the population performing a Fourier transformation to the time domain. The artificial effect introduced by the small imaginary part of the energy δ used to calculate the Green's function can be efficiently eliminated by multiplying the time evolution by $e^{+\delta t}$ (δ is positive).[46] We thus have

$$A_W(t) \approx A^{cut}_{isol}(t) = e^{+\delta t}\int_{-\infty}^{\infty} d\omega \tilde{A}^{cut}_{isol}(\omega) e^{-i\omega t}. \quad (24)$$

III. FIRST-PRINCIPLES CALCULATIONS

A. Slab calculations: Ru(0001) and Ar/Ru(0001)

We have performed most of our calculations with the SIESTA code,[34,35,47] which uses a basis set of numerical atomic orbitals and has been specially designed to deal with large systems. We use the local density approximation (LDA),[48] a supercell-slab geometry, and norm-conserving pseudopotentials. An 11×11 k sampling is used for slabs with 1×1 periodicity parallel to the surface, and a consistent sampling is used for larger supercells. For the geometrical optimizations, we have used the following basis sets: for Ru, a double-ζ basis (i.e., two different functions or radial shapes) to represent the 5s states, a single-ζ 4d shell, and a 5p polarization shell; for Ar, a double-ζ polarized basis set including a double-ζ basis to represent the 3s and 3p states and a single 3d polarization shell. For the rest of the calculations (with a fixed geometry) we have supplemented these basis sets with a 4f shell for Ru, and a double-ζ 4s shell and a single-ζ 4p shell for Ar. The radii of the orbitals were fixed with an *energy shift* of 100 meV.[49,50]

Our slabs contain typically between 9 and 11 metal layers plus a layer of Ar adsorbed both on the top and bottom surfaces. These thicknesses guarantee that the overlap and Hamiltonian matrix elements connecting the overlayers at both sides of the slab are strictly zero with the basis orbitals used here. In this way, as described in the previous section, we can unambiguously define those pieces of the Hamiltonian and overlap matrices associated with the atoms in each surface of the slab. The finite size effects associated with the finite thickness of the slab can affect the value of the matrix elements of the Hamiltonian in the surface region. However, we have checked that this effect is very small, and the calculations based on the slab containing 9 or 11 metal layers give identical results.

The lattice parameter in the lateral direction is fixed to that obtained for bulk Ru with our basis set[51] to avoid artificial stresses. Low energy electron diffraction (LEED) data indicate that Ar on Ru(0001) forms a roughly hexagonal, buckled layer on Ru(0001). The coverage is 0.5 relative to Ru, and the vertical Ar-Ru distances range between 3.0 (on top sites) and 3.3 Å.[52] The unit cell postulated in Ref. 52 contains six inequivalent Ar positions and 12 Ru atoms per substrate layer. Such a large unit cell would make some of our calculations difficult, particularly those to assess the convergence of the calculated charge transfer rates as a function of the concentration of excited Ar atoms in the layer. Instead, we have decided to consider two simplified systems corresponding to Ar coverages of 1 and 0.25, i.e., larger and smaller than the experimentally observed coverage. We have used hexagonal Ar layers commensurate with the substrate with lattice parameters equal to and twice that of Ru. Therefore, they correspond to 1×1 and 2×2 periodicities over the substrate. This approximation simplifies our calculations considerably and will be justified below, when we will see that, at least for the experimentally relevant Ru-Ar distance, the charge transfer time from a 4s resonance bound to an excited argon atom in the layer is weakly dependent on the Ar coverage. In fact, both Ar layers with 1×1 and 2×2 periodicities lead to an estimation of the charge transfer time in the range between 1 and 2 fs, in reasonable agreement with the experiment.[20]

We have started by studying the adsorption energies and geometries of these two Ar layers in Ru(0001). In principle, one could question such a study due to the lack of the van der Waals interactions in the current local and semilocal approximations to the density-functional theory. However, already more than two decades ago, Lang[53] showed that the local density approximation could correctly account for the adsorption of Ar on simple metal surfaces. Lang suggested that the interaction between Ar and the surface is dominated by a weak *chemical* interaction and thus can be described within LDA. More recent work[54] also showed that LDA can correctly describe the adsorption energy of Xe on transition metal surfaces, whereas the generalized gradient approximation (GGA) typically leads to a severe underestimation of the binding energies. This supports the idea that the usual overestimation of the chemical binding energy by LDA partially compensates the lack of dispersive interactions in many systems.

For the compressed 1×1 Ar layer, we find that the system relaxes to a metastable configuration (i.e., the system reduces its energy with respect to the freestanding 1×1 Ar layer although the adsorption energy with respect to the isolated Ar atom is negative) where the Ar atoms lie 3.14 and 3.33 Å above the Ru surface, respectively, for the on top and hollow (fcc and hcp) sites. For the more diluted 2×2 Ar layer, the calculated adsorption heights are 2.84, 2.94, and 2.97 Å, respectively, for the on top, the fcc, and the hcp configurations. Thus, our LDA Ru-Ar distances are shorter (by ~10% or less) than those measured with LEED.[52] This observation agrees with the results of Ref. 54 for the adsorption of Xe on various transition metal surfaces. Finally, for both Ar coverages, the distance between Ru layers is almost unchanged after the relaxation, except for the surface layer which suffers an inward relaxation of ~4% (this is quite similar for the clean or argon decorated surface). Experimentally, an inward relaxation of 2% is found for the clean surface; rare gas adsorption increases this contraction somewhat[55] but the effect of an Ar monolayer is very small.[52]

In our calculations, we have observed that Ar on top sites is more stable than fcc or hcp configurations. This is consis-

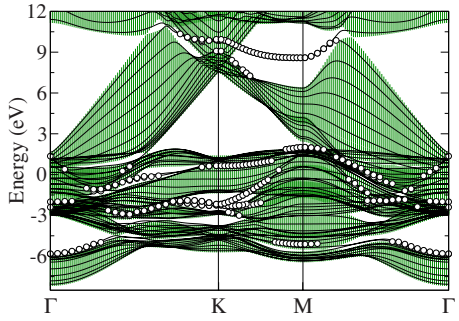

FIG. 2. (Color online) Band structure of the Ru(0001) surface. The solid lines are the bands of a slab of 11 layers, the vertical (green) bars represent the projected band structure of the bulk, and the open symbols show the surface states and resonances. The energies are referred to the Fermi level.

tent with all detailed LEED determinations,[55–57] as well as with the theoretical results for Xe on several transition metals [54] However, the binding energy of Ar on Ru(0001) is quite small and, therefore, difficult to determine accurately. In particular, one has to take into account that it can be severely influenced by the so-called basis set superposition error (BSSE).[58] The BSSE affects to a certain extent all calculations performed using atomic orbitals as a basis set (in general, all those using basis functions linked to the atomic positions), unless a fully saturated basis set is used. Since plane-wave calculations are not affected by the BSSE, we have repeated some of our calculations using a plane-wave code. We have used VASP.[59,60] The calculational parameters are similar to those used in Ref. 61, except that we use a seven layer Ru slab with symmetric Ar adsorption and the Perdew-Burke-Ernzerhof[62] functional when performing GGA calculations.[63] For the dilute 2×2 Ar adlayer, we find a binding energy of 106 meV (19 meV) and an adsorption height of 3.09 Å (4.16 Å) using LDA (GGA) for the on top sites. The adsorption energy predicted by LDA is in good agreement with the experimental determination by thermal desorption (100 meV).[64] Our GGA data are also in good agreement with the calculations of Feibelman,[61] who obtains a Ru-Ar distance of 4.4 Å and an adsorption energy of 24 meV for 1/12 Ar coverage using the PW91-GGA functional. The compressed 1×1 adlayer is bound to the Ru(0001) surface by 59 meV (~1 meV) at a distance over the substrate of 3.18 Å (4.24 Å). However, as mentioned above, the 1×1 adlayer is unstable against the desorption of Ar as an isolated atom. The "adsorption" energies are −655 meV (−998 meV).

In the following, we analyze the electronic structure of the structures obtained from our SIESTA LDA calculations (which are quite similar to those obtained with VASP). In Fig. 2, we show the band structure of the clean Ru(0001) surface calculated using our most complete basis set. The surface bands and surface resonances are marked with solid symbols, and the projection of the bulk band structure (vertical bars) has been superimposed to indicate the precise positions of the projected energy gaps. Surface states and resonances are identified via Mulliken population analysis[44] as those which possess a large weight in the surface layer (more than 40% in this case). While this procedure is not free from ambiguities, we find that it is a very simple way to identify surface related electronic features. Our band structure is in good agreement with that reported in the literature.[65] An interesting feature of this band structure is the presence of large projected band gaps that extend from a few eV above the Fermi energy up to quite high energies. Of particular importance for our results will be the projected band gap centered at the Γ point.

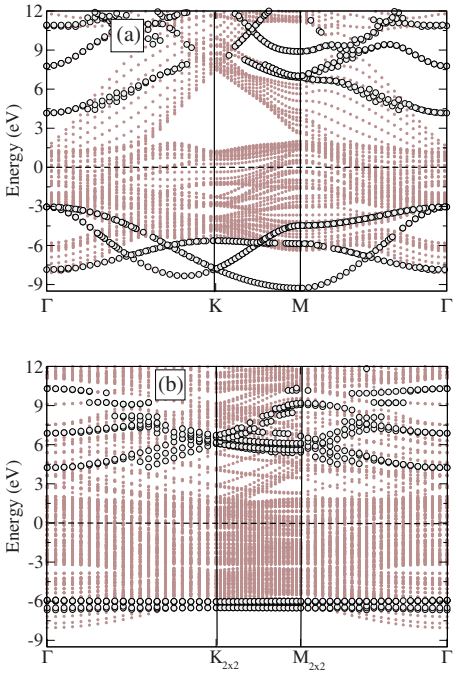

FIG. 3. (Color online) Band structure of the Ru(0001) surface covered by (a) a 1×1 adlayer and (b) a 2×2 adlayer of Ar atoms occupying on top adsorption sites. The dotted lines are the bands of a slab with 11 layers of Ru and a single adlayer of Ar on each of the surfaces, while the symbols highlight the bands with a strong weight in the Ar atoms. The energies are referred to the Fermi level.

In Figs. 3(a) and 3(b), we display the band structure of the Ru(0001) surface covered by Ar adlayers with 1×1 and 2×2 periodicities, with the Ar atoms occupying on top adsorption sites. Again, these band structures have been calculated with our most complete basis sets for both Ar and Ru. We can easily recognize the band complex due to the $3p$ states of Ar, located in the region centered 6 eV below the Fermi level. The lowest unoccupied band with Ar character comes mainly from the $4s$ states of Ar. The minimum of this band is located at very similar energies for both adlayers (4.16 and 4.23 eV above the Fermi level, respectively, for the 1×1 and the 2×2 periodicities). The Ar $4s$ band presents an almost identical paraboliclike dispersion for both layers. When the Ar atoms are located in other adsorption sites, the band structure remains almost unchanged. For example, comparing the band structures for fcc and "on top" adsorption sites, we only find a rigid shift of the Ar bands of a few tenths of eV to higher energies in the former case. For the hcp adsorption, the band structure is almost identical to the fcc case. This seems to indicate that this energy shift is primarily a function of the Ar height over the substrate for a given Ar coverage.

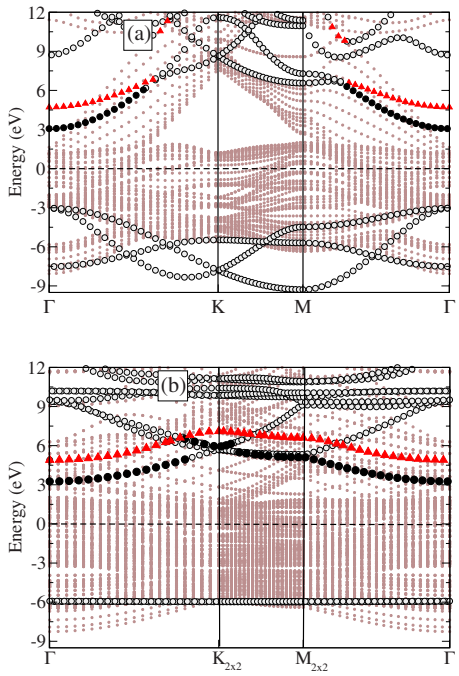

FIG. 4. (Color online) Superimposed band structures of the clean Ru(0001) surface [dotted lines, data in panel (a) also displayed in Fig. 2] and of isolated hexagonal layers of Ar (symbols), with (a) the same lattice parameter as the substrate and (b) twice the Ru lattice parameter. Two bands of the layers have been highlighted: (i) states with more than a 50% weight in the 4*s* states of Ar (black circles) and (ii) states with more than a 50% weight in the 4_{p_z} states of Ar (red triangles).

Due to the relatively large distance between the Ar atoms and the Ru substrate, and the closed-shell character of Ar, we can expect the band structures of the adsorbed layers to be closely related to those of isolated hexagonal Ar layers with the same lattice parameters. In Fig. 4, we check that this is indeed the case. Here, we have superimposed the band structures calculated independently for the clean Ru(0001) surface and for isolated hexagonal layers of Ar with a nearest-neighbor distances of 2.702 and 5.404 Å, similar to those of the adsorbed layers. The two independent band structures are aligned so that the top of the 3*p* band complex is located at the same energy, relative to the Fermi level, as that for the combined system. Two bands of the Ar layers have been highlighted: (i) those states with more than a 50% weight in the 4*s* states of Ar and (ii) those states with a weight of more than 50% in the $4p_z$ states of Ar.

The similarities between Figs. 3 and 4 are evident. The Ar 3*p* bands have exactly the same topology and almost the same width in the case of the isolated and the supported 1×1 layer. This indicates that, at least for this compressed layer with the same lateral lattice parameter as the substrate, the interaction between Ar neighbors ($d_{\text{Ar-Ar}}=2.702$ Å) is larger than the interaction between Ar and Ru ($d_{\text{Ru-Ar}}=3.14$ Å). On the other hand, the 3*p* bands of the adsorbed 2×2 adlayer have a width of ~0.7 eV due to the interaction with the substrate, while such width is as small as ~0.03 eV for the isolated 2×2 layer. Again, this is consistent with the distances $d_{\text{Ru-Ar}}=2.84$ Å and $d_{\text{Ar-Ar}}=5.404$ Å.

The most noticeable differences between the band structures displayed in Figs. 3 and 4 can be found in the unoccupied part of the spectrum. The unoccupied bands are shifted to higher energies in the case of the deposited Ar layers relative to the freestanding cases. This is clear in the case of the lowest unoccupied Ar band (4*s* band), whose minimum has been raised by ~1 eV. This shift is larger in the case of the $4p_z$ band, which in Figs. 4(a) and 4(b) appears only ~1.7 eV above the 4*s* band, while in Figs. 3(a) and 3(b), it is found, respectively, at 7.8 and 6.9 eV above the Fermi level (i.e., ~3.6 and 2.6 eV above the 4*s* band). These upward shifts of the conduction bands can be interpreted as a result of the additional confinement associated with the presence of the neighboring Ru surface. This effect is accompanied by an important hybridization between the 4*s* and $4p_z$ states of Ar.

We can summarize the main observations of this section: (i) the band structure of Ar/Ru(0001) depends very weakly on the adsorption site; (ii) the band structures of the supported and freestanding Ar layers are very similar, although (iii) the conduction bands of the Ar adlayer suffer shifts to higher energies due to the extra confinement provided by the proximity of the Ru substrate and the shift is larger for the bands derived from the $4p_z$ Ar states; (iv) the position and dispersion of the Ar 4*s* band seem to be weakly dependent on the Ar coverage. Points (i) and (iv) justify our use of idealized structures for the Ar adlayer with simple unit cells commensurate with the substrate and corresponding to coverages different from the complex experimental structure.[52] In general, we find that the positions of the argon levels depend on the distance between the Ar adlayer and the Ru surface. As we will see below, this has important consequences for the behavior of the charge transfer time as a function of the Ru-Ar distance.

B. Excited Ar atoms

In the experiments that we want to address,[20] the Ar/Ru(0001) system is irradiated with soft x rays with energies in the range of the resonant transition between the $2p_{3/2}$ level and the 4*s* bound resonance of Ar. As a consequence, some of the Ar atoms in the adlayer are excited to a $2p_{3/2}^{-1}4s^{+1}$ configuration. Our next step is to perform density-functional calculations that mimic this situation, i.e., some of the Ar atoms in the layer are substituted by $\text{Ar}^{\star}(2p_{3/2}^{-1}4s^{+1})$. From these self-consistent calculations, we will obtain a corrected position of the 4*s* level, including some of the effects of the electronic relaxation in the excited $\text{Ar}^{\star}$ atoms and their neighbors, and the effective LDA Hamiltonian to describe the charge transfer dynamics from the 4*s* resonance into the substrate. Both processes, the excitation and the subsequent charge transfer to the substrate, take place on a time scale smaller than that of atomic relaxations. Therefore, in what follows, the geometries are kept to those obtained for the ground state of an Ar layer on Ru(0001). Only $d_{\text{Ru-Ar}}$ will be changed in the range from 6 to 3.14 Å, in order to explore the effect of this parameter on the charge transfer time.

We perform calculations with different concentrations (x) of photoexcited $\text{Ar}^{\star}$ atoms. For this purpose, it is necessary

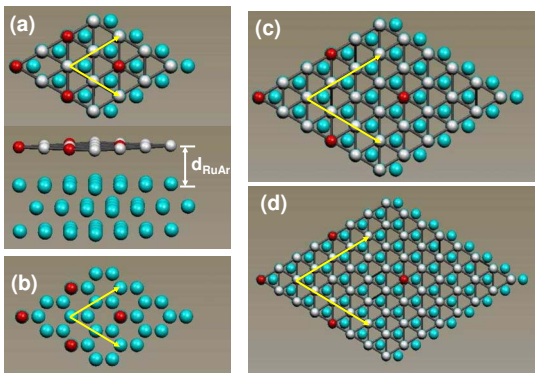

FIG. 5. (Color online) Summary of the different systems studied in this paper. Large (blue) spheres represent ruthenium atoms. Light gray and dark (red) smaller spheres represent Ar and Ar* atoms, respectively. The supercell lattice vectors are also depicted. (a) 2×2 supercell corresponding to an $Ar^\star Ar_3$ adlayer ($x=1/4$). The distance between the surface and the argon layer $d_{Ru\text{-}Ar}$ varies between 3.14 Å (equilibrium distance found in the calculations) and 6 Å. The lattice parameter within this Ar layer is equal to that of the Ru surface. An equivalent system with two argon layers was also studied (not shown). We also calculated a more diluted 2×2 system (b) containing only excited adsorbates [Ru(0001)-(2×2)-Ar*]. The lattice constant within this diluted layer is twice that of the substrate. (c) 3×3 supercell ($Ar^\star Ar_8$ adlayer, $x=1/9$). (d) 4×4 supercell ($Ar^\star Ar_{15}$ adlayer, $x=1/16$).

to construct supercells along the lateral directions. We have considered sizes up to 4×4, in units of the surface Ru unit cell, corresponding to $x=1/16$ and slabs containing 176 atoms. We mostly concentrate on the compressed Ar layer with

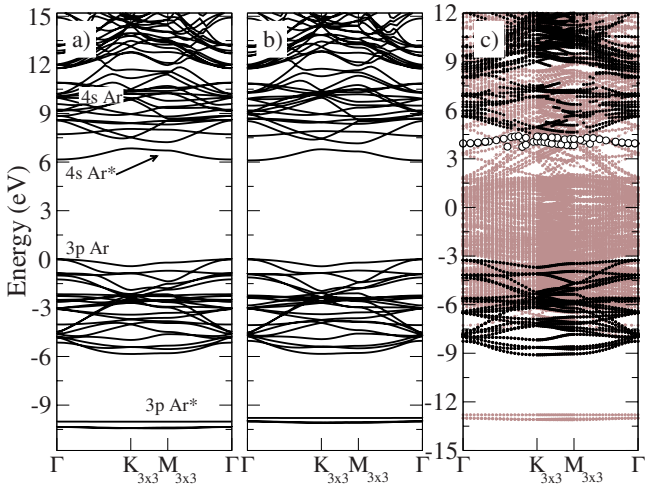

FIG. 6. (Color online) (a) "Exact" band structure of an isolated $Ar^\star Ar_8$ layer ($d_{Ar\text{-}Ar}=2.702$ Å), i.e., containing one photoexcited atom out of every nine. (b) The same isolated layer calculated using the frozen $4s$ approximation. Energies are referred to the top of the $3p$ Ar complex. (c) Band structure of the $Ar^\star Ar_8$/Ru(0001) combined system using the frozen $4s$ approximation described here. Black symbols indicate states with main character on the Ar atoms. Open symbols are states with primary Ar* $4s$ character. For (a) and (b), energies are referred to the top of the $3p$ Ar complex. For (c), energies are referred to the Fermi level.

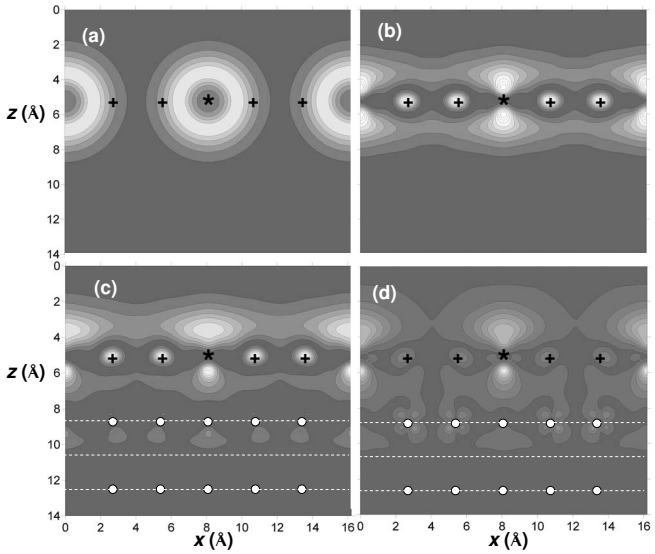

FIG. 7. (a) Density associated with the $4s$ orbitals of the Ar* atoms and (b) with the eigenfunction of the $4s$ Ar* band at Γ of an isolated $Ar^\star Ar_8$ layer ($d_{Ar\text{-}Ar}=2.702$ Å). (c) and (d) show the density obtained after projecting the $4s$ Ar* eigenfunctions of the isolated layer at Γ and K into the unoccupied states of the combined $Ar^\star Ar_8$/Ru(0001) system. Crosses represent schematically the position of the Ar atoms, and stars the position of the Ar* atoms in the layer. Circles and lines represent the position of the Ru atoms and Ru planes.

an Ar-Ar distance of 2.702 Å, equal to the Ru-Ru distance in the substrate. However, we also present one set of calculations for a more diluted system with $d_{Ar\text{-}Ar}=5.404$ Å. A summary of the studied systems can be found in Fig. 5. The Ar* pseudopotential contains a hole in the $2p_{3/2}$ level and is quite similar to that of K. Thus, our calculations assume that the core-hole lifetime is much longer than the time required for the relaxation of the valence electrons, which is a reasonable assumption for a metallic substrate.[66]

Figure 6(a) shows the self-consistent band structure for an isolated hexagonal Ar layer with one atom out of every nine ($Ar^\star Ar_8$, $d_{Ar\text{-}Ar}=2.702$ Å) excited. As expected, the excited electron remains attached to the Ar* atom, and the $4s$ resonance forms an impurity level within the band gap of the layer. The electron density associated with this level at Γ is shown in Fig. 7(b). It deviates from a simple superposition of $4s$ Ar* orbitals [see panel (a)]. The effect of the Ar neighbors and the hybridization with the $4p_z$ Ar* states is evident in the figure. The wave functions of the $4s$ impurity band will provide the wave packets $\Psi_R(\mathbf{k}_\parallel)$ used to project the Green's function. This choice will be further justified below.

Notice that, although physically we represent an excited state, indeed we perform a "ground-state" calculation for a system containing two species, Ar and Ar*. Unfortunately, this procedure only works for an isolated layer. For the adsorbed layer, the $4s$ electron will be transferred into the metal slab during the self-consistent calculation. Thus, it will fail to describe our initial configuration where the electron is *still* attached to the Ar*. For this reason, we need to make an approximation: The self-consistent calculation is performed under the constraint that the electron remains confined to an

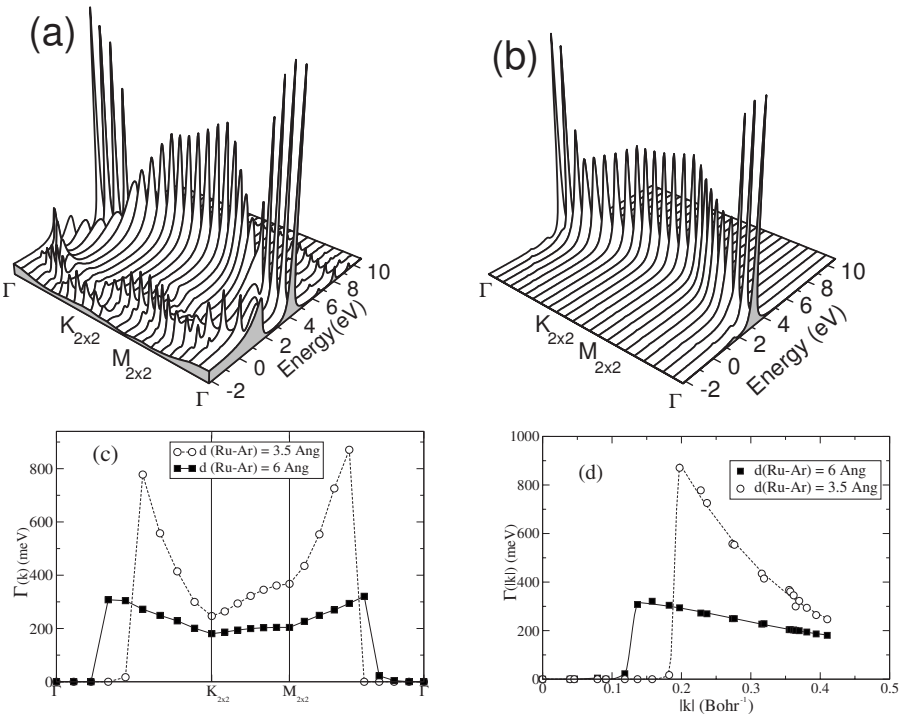

FIG. 8. (a) Imaginary part of the projected Green's function $\mathrm{Im}[G_{RR}(\omega,\mathbf{k}_\parallel)]$ for the 2×2 supercell system [see panel (a) in Fig. 5] and 3.5 Å separation between the $Ar^\star Ar_3$ adlayer ($d_{\mathrm{Ar\text{-}Ar}}=2.702$ Å) and the Ru substrate as a function of $\mathbf{k}_\parallel$ and the energy (energies referred to the Fermi energy). (b) The same for $d_{\mathrm{Ru\text{-}Ar}}=6$ Å. (c) The corresponding values of $\Gamma(\mathbf{k}_\parallel)$ as a function of $\mathbf{k}_\parallel$ in the supercell Brillouin zone and (d) as a function of $k_\parallel$, the modulus of $\mathbf{k}_\parallel$.

atomiclike 4*s* state associated with the $Ar^\star$ atom. The remaining electrons are allowed to accommodate to the presence of the excited adsorbate. We call this the "frozen 4*s*" approximation. This is consistent with the notion that the characteristic time for building up the screening in the metal is much shorter than the charge transfer time. Indeed, the screening time is of the order of a few tenths of a femtosecond for typical metallic densities as shown, for example, by recent time-dependent density-functional calculations.[66] More precisely, with N_e the total number of electrons in our symmetric supercell-slab calculation, the electronic density is constructed as

$$\rho(\mathbf{r}) = \rho_{SCF}^{(N_e-2)}(\mathbf{r}) + \rho_{4s}(\mathbf{r}-\mathbf{R}_U) + \rho_{4s}(\mathbf{r}-\mathbf{R}_L)$$
$$= 2\sum_{i=1}^{(N_e-1)/2} |\Phi_i(\mathbf{r})|^2 + \rho_{4s}(\mathbf{r}-\mathbf{R}_U) + \rho_{4s}(\mathbf{r}-\mathbf{R}_L), \tag{25}$$

where $\Phi_i(\mathbf{r})$ are the $(N_e-1)/2$ lowest solutions of the Kohn-Sham-like equations

$$H^{LDA}[\rho(\mathbf{r})]\Phi_i(\mathbf{r}) = \epsilon_i\Phi_i(\mathbf{r}), \tag{26}$$

$\rho_{4s}(\mathbf{r})$ is the density corresponding to an atomic 4*s* state of the $Ar^\star$ atom populated with one electron, and $\mathbf{R}_U$ and $\mathbf{R}_L$ are the positions of the $Ar^\star$ atoms in the upper and lower surfaces of the slab, respectively. According to Figs. 7(a) and 7(b), the choice of an atomic density for $\rho_{4s}(\mathbf{r})$ is not optimal. However, this approximation already produces very good results and more sophisticated schemes have not been pursued here.

Figures 6(b) and 6(c) depict the results of the approximate calculation for an isolated and adsorbed $Ar^\star Ar_8$ layer ($d_{\mathrm{Ru\text{-}Ar}}=3.14$ Å), respectively. Panels (a) and (b) are almost identical, justifying the use of this scheme. In panel (c), we have identified the bands with main Ar and $Ar^\star$ content by means of a Mulliken population analysis.[44] The bands in (c) are very similar to a superposition of the band structure of the surface and the isolated layer, consistent with the relatively weak adsorbate-substrate interaction that can be expected for noble gases and the results presented in the previous section. Again, we can see the overall upward shift of the unoccupied Ar and $Ar^\star$ states. The minimum of the 4*s* $Ar^\star$ band appears at 3.95 eV above the Fermi energy, which compares reasonably well with the measured 3.4 eV.[20]

Finally, we need to check that the wave functions of the 4*s* $Ar^\star$ band of the isolated layer are indeed a suitable choice for the wave packets $\Psi_R(\mathbf{k}_\parallel)$ used to project the Green's function of the supported system. This is justified by the data in Figs. 7(c) and 7(d). They show, at the Γ and K points of the supercell surface Brillouin zone, the density associated with the wave packets obtained after projecting $\Psi_R(\mathbf{k}_\parallel)$ into the unoccupied states (up to 7 eV above E_F) of the combined Ar/Ru(0001) system. The supported and freestanding cases are quite similar. The main differences are a moderate shift of the density toward the vacuum region and a small hybridization with the Ru atoms in the surface layer in the former case. Indeed, only ~20% of the norm of the $\Psi_R(\mathbf{k}_\parallel)$ wave packets is lost during the projection process, showing that they have a large overlap with the wave functions of the true 4*s* resonance band present in this energy range.

IV. DYNAMICS OF THE 4*s* $Ar^\star$ RESONANCE IN Ar/Ru(0001)

A. Resonance width: dependence on the Ru-Ar distance

In Fig. 8, we show $\mathrm{Im}[G_{RR}(\omega,\mathbf{k}_\parallel)]$ for two distances between the overlayer and the surface $d_{\mathrm{Ru\text{-}Ar}}$ (3.5 and 6 Å) and

a concentration of Ar* atoms of $x=1/4$. Both sets of data are dominated by a main peak that can be identified with the band associated with the 4*s* resonance of the Ar* atoms. For the smallest Ru-Ar distance, close to the experimental value, we also find other peaks associated with surface bands and resonances of the Ru(0001) surface. This is an indication of a stronger adsorbate-substrate interaction and hybridization. One of these surface resonances maps the boundary of the projected band gap. This surface resonance originates from the *s* and p_z Ru states and is very similar to the surface state that appears in the (111) surfaces of the noble metals. In panels (c) and (d), we show the width of the Ar* resonance peak obtained following the fitting procedure described in Sec. II B. The data are calculated along the $\Gamma-K_{2\times2}$, $K_{2\times2}-M_{2\times2}$, and $M_{2\times2}-\Gamma$ directions of the supercell Brillouin zone. Other directions are quite similar due to the hexagonal symmetry of the system, and $\Gamma(\mathbf{k}_\parallel)$ can be described as a function of $k_\parallel$, the modulus of $\mathbf{k}_\parallel$. This becomes clear in Fig. 8. Following the recipe described in Sec. II B we can obtain from these data the effective width of the 4*s* resonance for an isolated excited argon atom:

$$\Gamma_{isol}^{\mathrm{Ar}^\star 4s} \approx \frac{A_{SC}}{(2\pi)^2}\int_{SBZ} dk_\parallel^2 S_{4s^\star,4s^\star}(k_\parallel)\Gamma(k_\parallel), \qquad (27)$$

where the integration is performed over the supercell Brillouin zone (SBZ) and A_{SC} is the area of the supercell. Notice that due to the spherical symmetry of the *s* orbital, the overlap $S_{4s^\star,4s^\star}$ only depends on $k_\parallel$. Furthermore, for supercells larger than 2×2, it becomes identically 1, independent of $k_\parallel$. Figure 8 shows a sharp reduction of $\Gamma(k_\parallel)$ for small values of $k_\parallel$. Near the Γ point, the width of the resonance becomes negligible. This is a clear consequence of the existence of a band gap in the projected band structure of bulk Ru around Γ (see Fig. 2), in spite of the band folding associated with the doubling of the periodicity in real space. For small values of $k_\parallel$, there are fewer bulk states available for decay and they couple less efficiently to the corresponding levels of the argon adlayer. The gap eventually disappears for the energy range of interest when we move away from Γ, and the peaks develop a finite width.

Figure 9(a) shows the results of the evaluation of Eq. (27) as a function of the distance between the adlayer and the metallic surface for supercells of several sizes (i.e., different concentrations *x* of photoexcited Ar* atoms). Surprisingly, the effective width $\Gamma_{isol}^{\mathrm{Ar}^\star 4s}$ does not decay monotonously with $d_{\mathrm{Ru\text{-}Ar}}$. This behavior can be understood as the result of two competing effects with opposite impact in $\Gamma_{isol}^{\mathrm{Ar}^\star 4s}$ as $d_{\mathrm{Ru\text{-}Ar}}$ increases: (i) the expected decrease of the width of the peaks $\Gamma(k_\parallel)$ as a consequence of the reduction of the interaction matrix elements between the adlayer and the substrate and (ii) the shift to lower energies of the resonance when the Ru-Ar distance is increased. The latter effect can be seen in detail in Fig. 9(b). The shift is due to the extra confinement of the 4*s* Ar* state when the atom approaches the substrate and is enhanced by the polarization of the metallic surface.[67,68] The presence of this upward shift of the unoccupied states of the deposited argon layer was already pointed out in the description of our first-principles calculations in the previous section. The shift of the resonance energy translates into a different impact of the substrate projected band gap in the final results [since the gap affects regions of different sizes of the supercell Brillouin zone in the integral in Eq. (27)]. Thus, effect (i) tends to decrease $\Gamma_{isol}^{\mathrm{Ar}^\star 4s}$ as $d_{\mathrm{Ru\text{-}Ar}}$ increases, whereas effect (ii) tends to increase it. The complex behavior of the curves arises from this competition. The two competing effects can also be noticed in the data in Fig. 8(d).

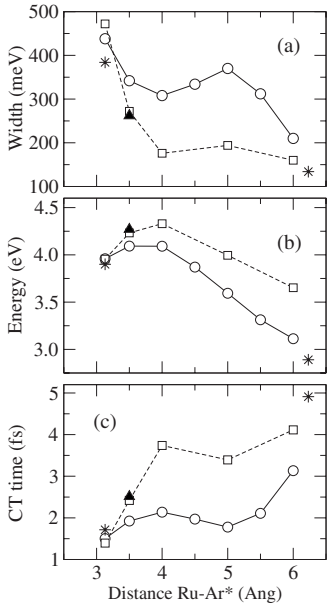

FIG. 9. (a) $\Gamma_{isol}^{\mathrm{Ar}^\star 4s}$ as a function of the distance between an argon adlayer with a lattice parameter $d_{\mathrm{Ar\text{-}Ar}}=2.702$ Å and the ruthenium surface. (b) Position, referred to E_F, of the Ar* 4*s* resonance band minimum. (c) Charge transfer time, $\tau_{CT}=(\Gamma_{isol}^{\mathrm{Ar}^\star 4s})^{-1}$. Circles, squares, and triangles stand, respectively, for the data obtained using 2×2, 3×3, and 4×4 supercells ($x=1/4, 1/9, 1/16$). The stars show the data obtained for an argon bilayer using a 2×2 lateral supercell. Two situations are studied, with one excited Ar* atom in the lower and the upper layer, respectively.

The behavior of the energy and width of the 4*s* Ar* resonance in Ar/Ru(0001) depicted in Figs. 9(a) and 9(b) is very similar to that of the model calculation by Gauyacq and Borisov[68] for the Ar/Cu(111) system. They also resemble the results obtained by Borisov *et al.*,[67] again using a simplified description of the electronic structure of the substrate, for the case of alkali atoms on Cu(111). The importance of the projected band gap in determining the magnitude and distance dependence of the resonant charge transfer rates was also pointed out for that system.

Figure 9(a) also shows the convergence of our calculations of $\Gamma_{isol}^{\mathrm{Ar}^\star 4s}$ as a function of the lateral size of the supercell. For distances in the range 3.0–3.5 Å, all the calculations give similar numbers. However, for larger Ru-Ar distances, the results obtained with 2×2 and 3×3 supercells start to deviate significantly. This is a consequence of the different position of the minimum of the Ar* 4*s* band within the ruthenium projected band gap [see Fig. 9(b)]. For a Ru-Ar distance of 3.5 Å, we have also performed a calcula-

TABLE II. Calculated charge transfer times (τ_{CT}) as a function of the distance between an Ar adlayer with lattice parameter $d_{\text{Ar-Ar}}$=2.702 Å and the metallic surface $d_{\text{Ru-Ar}}$, using supercells of different sizes.

	τ_{CT} (fs)		
$d_{\text{Ru-Ar}}$ (Å)	2×2	3×3	4×4
6.0	3.14	4.11	
5.5	2.11		
5.0	1.78	3.39	
4.5	1.97		
4.0	2.14	3.74	
3.5	1.92	2.42	2.51
3.14	1.50	1.39	

tion using a larger supercell with 4×4 periodicity. The results are almost identical to those obtained with a 3×3 supercell indicating that, at least for this distance, we have a converged value of the $\Gamma_{isol}^{\text{Ar}^\star\ 4s}$.

So far, we have used Eq. (27) to calculate $\Gamma_{isol}^{\text{Ar}^\star\ 4s}$. However, at the end of Sec. II B we outlined a different procedure to obtain the effective width of the isolated resonance from our periodic calculations. The idea is to extract the width from an analysis of the function $\tilde{A}_{isol}(\omega)$ [given in Eq. (21)]. In Table I, we can see that both methods give very similar results. However, we normally prefer the use of Eq. (27) since it makes it easier to take into account the presence of other surface states and resonances not directly related to the $\text{Ar}^\star$ 4*s* level, in order to extract reliable values of the width, considering each $k_\parallel$ independently.

The charge transfer time can be obtained using the relation $\tau_{CT}=(\Gamma_{isol}^{\text{Ar}^\star\ 4s})^{-1}$. The data are shown in Fig. 9(c) and in Table II. Our estimated charge transfer times for the experimentally relevant Ru-Ar distances, using our compressed model of the Ar layer, range between 1.4 and 2.5 fs. In the following, we will see that our more diluted Ar layer [Ru(0001)-(2×2)-$\text{Ar}^\star$] provides a slightly smaller value of 1 fs, due to the shift to lower energies by several tenths of eV of the $\text{Ar}^\star$ 4*s* resonance. These data are in reasonable agreement with the experimental value of 1.5 fs at resonance (varying from 1.2 fs below the resonance to 2.0 fs above it) obtained using resonant Auger spectroscopy.[20] We should point out, however, that our calculation only takes into account the resonant charge transfer as a source of decay for the 4*s* $\text{Ar}^\star$ level. Other sources of decay are inelastic processes due to electron-electron and electron-phonon scattering. They typically take place over longer time scales. For example, in the case of alkali atoms on Cu(111), the inelastic decay rate due to electron-electron scattering has been estimated to be in the range $\Gamma_{ee}\approx 15-22$ meV.[69] Adding this value to the total width, we get a quite small correction of the calculated decay times, which are reduced by ~0.1 fs for a 3.5 Å separation and ~0.3 fs for 6 Å.

In Fig. 9, we also show the data obtained for an argon bilayer calculated using a 2×2 supercell. The lower argon layer is situated at 3.14 Å from the Ru(0001) surface and the upper at 6.23 Å. The corresponding charge transfer times are 1.71 and 4.9 fs. The resonance is shifted by approximately 1.0 eV to lower energies when the excited $\text{Ar}^\star$ is located in the upper layer with respect to its position when the $\text{Ar}^\star$ lies in the lower layer. This follows the trend already observed for the position of the level as a function of the Ru-Ar distance for the case of just one argon layer. The values obtained for the charge transfer times are also very similar to those computed for a single layer. This indicates that the lower argon layer acts mainly as a separator, increasing the distance between the excited atom and the metallic surface, when the excited $\text{Ar}^\star$ atom is located in the upper layer. The observed downward shift of the $\text{Ar}^\star$ 4*s* level and the increase of the charge transfer time are consistent with the trends observed in Ref. 20 when a Xe layer was used as a separator between Ar and the metallic surface.

B. Resonance width: Dependence on its energy position and on the Ar coverage

We have seen that the position of the $\text{Ar}^\star$ 4*s* level relative to the projected band gap of ruthenium is crucial to determine its effective width and charge transfer time. Unfortunately, in the calculations presented in Fig. 9, this effect is entangled with the effect associated with the variation of the distance between the argon layer and the surface. In Fig. 10(a), we present some data for $\Gamma_{isol}^{\text{Ar}^\star\ 4s}$ as a function of the energy position of the $\text{Ar}^\star$ 4*s* resonance at a fixed value of $d_{\text{Ru-Ar}}$. To perform this study, we shifted the position of the levels associated with the $\text{Ar}_x^\star\text{Ar}$ layer relative to those of the Ru substrate. In order to do this, we modified the electronic Hamiltonian in the following way:

$$\tilde{H}_{\mu\nu}=\begin{cases} H_{\mu\nu}-\Delta\epsilon S_{\mu\nu} & \text{if } \mu,\nu\in \text{Ar}_x^\star\text{Ar} \\ H_{\mu\nu} & \text{if } \mu,\nu\notin \text{Ar}_x^\star\text{Ar}. \end{cases} \tag{28}$$

$H_{\mu\nu}$ and $S_{\mu\nu}$ are, respectively, the calculated LDA Hamiltonian and the overlap between the atomic orbitals used as a basis set. $\tilde{H}_{\mu\nu}$ is the new Hamiltonian. This procedure assumes that the states of the combined system can be considered as either mainly Ar or mainly Ru states, which is a reasonable assumption due to the small coupling between the argon system and the metallic substrate. In principle, only the Ar states are shifted in Eq. (28) by $\Delta\epsilon$, while the interaction with the metallic substrate is left unchanged. The procedure is approximate but allows exploring the effect of the energy position of the resonance in the charge transfer time. We can see in Fig. 10(a) a roughly linear decrease of the width of the $\text{Ar}^\star$ 4*s* resonance as the level is shifted upward from its initial position at ~4.16 eV (referred to E_F). This behavior is expected due to the existence of a band gap in the projected band structure of Ru(0001). This effect is consistent with the experimental observation in Ref. 20 that larger Raman fractions of the $\text{Ar}^\star(2p^{-1}4s^{+1})$ autoionization process are obtained by pumping the initially excited electrons to higher energies across the $\text{Ar}^\star$ 4*s* resonance on Ar/Ru(0001). According to the usual interpretation of core-hole-clock spectroscopy data, this leads to larger charge transfer times for electrons at higher energies. A similar re-

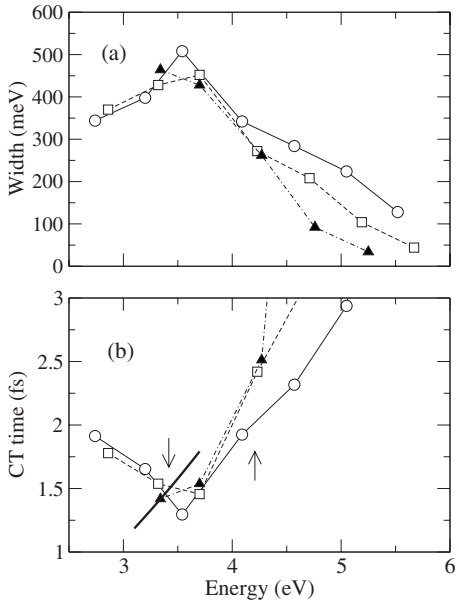

FIG. 10. (a) $\Gamma_{isol}^{Ar^\star 4s}$ as a function of the energy, referred to E_F, of the $Ar^\star$ $4s$ band minimum (at the Γ point) for a fixed Ru-Ar distance of 3.5 Å. The levels of the $Ar_x^\star Ar$ layers ($d_{Ar\text{-}Ar}$=2.702 Å) have been shifted with respect to those of the metallic substrate using Eq. (28). The corresponding charge transfer times τ_{CT} are shown in (b) compared with the experimental data (thick solid line) from Ref. 20. Circles, squares, and triangles stand, respectively, for the data obtained using 2×2, 3×3, and 4×4 supercells ($x=1/4,1/9,1/16$). The arrows in panel (b) indicate the position of the resonance in the experiment (~3.4 eV above E_F) and the calculated $Ar^\star$ $4s$ level (~4.1 eV above E_F) for $d_{Ru\text{-}Ar}$=3.5 Å.

sult has been found for Ar on Cu(111), Ag(111), and Ni(111) in Ref. 22. This behavior is very difficult to understand in a model where the electrons tunnel into a free-electron-like metal (i.e., with a featureless density of states) through an energy barrier. However, it can be easily understood from the reduction of the available phase space due to the presence of the projected band gap in the electronic structure of the substrate near Γ. This is indeed a common feature for all the metallic surfaces listed above. Thus, a possible explanation for the experimental observation is as follows. There are many different adsorption sites for $Ar^\star$ due to the varying registry between the Ru substrate and the Ar layer, different arrangements of the Ar neighbors around a given photoexcited $Ar^\star$, and the presence of defects in the surface. Each of these different sites is characterized by a slightly different binding energy of the $Ar^\star$ $4s$ level. As we change the excitation energy, we resonantly excite different $Ar^\star$ atoms and obtain a variation of the charge transfer time that maps the position of the corresponding $4s^\star$ level in the projected band gap. This seems to be consistent with the observation of a slightly broadened and quite asymmetric[22] resonance peaks in the x-ray absorption spectra of Ar on Cu, Ag, and Ni (111) surfaces.[22] This explanation of the reported change in the measured charge transfer time with the photon energy was already proposed by Gauyacq and Borisov in Ref. 68. The application of this model to the case of Ar on Ru(0001) is more problematic since the adsorption peaks do not show appreciable inhomogeneous broadening in this case. However, our results seem to indicate that also for Ar/Ru(0001), the observed variation stems from the energy and momentum dependence of the final states in the metal. A comparison between the behavior of the charge transfer times found in the experiment and in our calculations can be found in Fig. 10(b). Although the calculated and observed positions of the resonance peak are somewhat different, the charge transfer time dependence on the electron energy is quite similar in both cases.

In Fig. 10(a), we can observe that the width has a maximum for a resonance position around ~3.5 eV. This is not a signature of the disappearance of the projected band gap that only closes at ~1.7 eV above E_F. Looking at the band structure in Fig. 2, we cannot find any clear change in the nature of the Ru states at this energy that justifies such behavior. To understand the origin of this behavior, we have to take into account in more detail the dependence of the width on the available phase space at a given energy and how this is modulated by the dependence of the interaction matrix elements on $k_\parallel$. We can explore this using a very simple model. According to Eq. (4), the width of the level at a given energy ϵ_{4s} is given by

$$\Gamma^{Ar^\star 4s}(\epsilon_{4s}) = 4\pi^2 \int_{k_{min}(\epsilon_{4s})}^{k_{max}(\epsilon_{4s})} dk_\parallel k_\parallel |V_{4s}(k_\parallel)|^2, \tag{29}$$

where $V_{4s}(k_\parallel)$ is the interaction between the wave packet of the localized resonance and the electronic states in the substrate with a given crystalline momentum $\mathbf{k}_\parallel$. Due to the presence of a band gap at Γ, for a given value of the energy ϵ_{4s}, the available values of $k_\parallel$ are between a certain $k_{min}(\epsilon_{4s})$ and a $k_{max}(\epsilon_{4s})$ value. Inspecting the band structure of Ru(0001) in Fig. 2 along the Γ-K, for instance, we can find these values. Therefore, the integration window in Eq. (29) shifts as a function of ϵ_{4s}. To proceed further, we can simply assume that the interaction matrix element is proportional to the overlap between the $Ar^\star$ $4s$ orbital and the wave functions of the substrate,

$$\begin{aligned} V_{4s}(k_\parallel) &\sim \int dr^3 \psi_{\mathbf{k}_\parallel}(\mathbf{r}_\parallel, z)\phi_{4s}(\mathbf{r}) \\ &\sim \psi_{\mathbf{k}_\parallel}(0, d_{Ru\text{-}Ar}) \int dr_\parallel^2 dz e^{-i\mathbf{k}_\parallel\cdot\mathbf{r}_\parallel}\phi_{4s}(\mathbf{r}) \\ &\sim f(d_{Ru\text{-}Ar}, k_\parallel) \times \tilde{\phi}_{4s}(k_\parallel). \end{aligned} \tag{30}$$

ϕ_{4s} is the $4s$ orbital of an excited $Ar^\star$ atom and $\tilde{\phi}_{4s}(k_\parallel)$ its Fourier transform. $f(d_{Ru\text{-}Ar}, k_\parallel)$ is a function of the distance between the Ar atom and the surface and $k_\parallel$, which for small values of $d_{Ru\text{-}Ar}$ should have a relatively weak dependence on $k_\parallel$. However, for large values of $d_{Ru\text{-}Ar}$, it may be approximated by

$$f(d_{Ru\text{-}Ar}, k_\parallel) \approx \exp[-(d_{Ru\text{-}Ar} - d_0)\sqrt{\Phi - \epsilon_{4s} + k_\parallel^2/2m^\star}], \tag{31}$$

with Φ the surface work function, $m^\star$ the effective mass of the Ru bands, and d_0 the distance at which the exponential

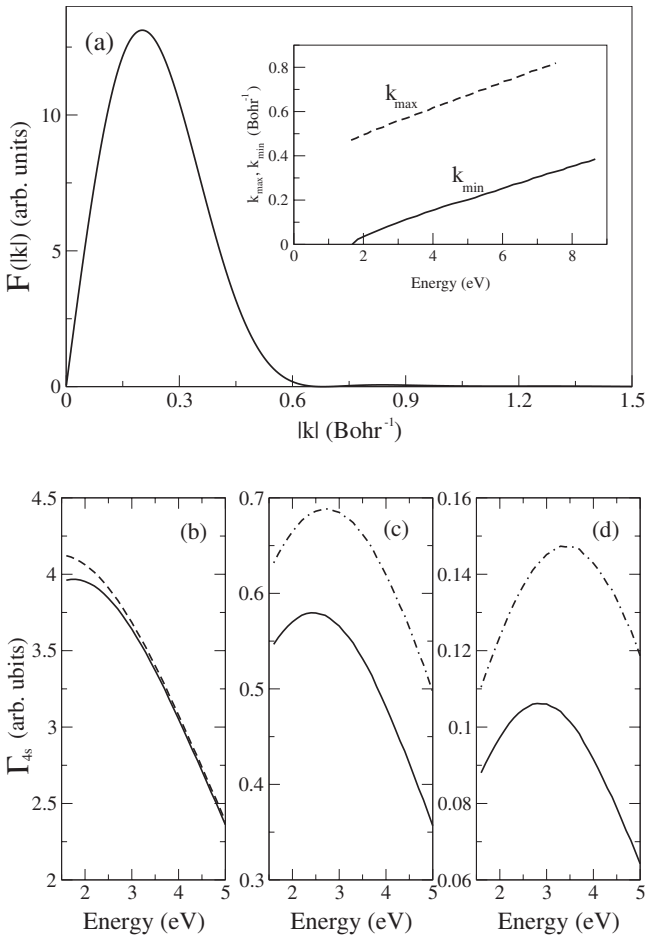

FIG. 11. Simple model for the energy dependence of the resonance width. (a) $F(k_\parallel)=k_\parallel|\tilde{\phi}_{4s}(k_\parallel)|^2$. $\tilde{\phi}_{4s}(k_\parallel)$ is the Fourier transform of the 4*s* pseudoatomic orbital of the Ar* atom used as a basis function in our calculation. The inset shows k_{max} and k_{min} as a function of the energy (as obtained from the Γ-K dispersion of the ruthenium bands). Panels (b), (c), and (d) show the behavior of $\Gamma^{\mathrm{Ar}^\star\,4s}$ given by Eq. (32) using different parameters. (b) The solid line shows the results with $f(d_{\mathrm{Ru\text{-}Ar},k_\parallel})=1$; for the dashed line, we additionally take $k_{max}\to\infty$. (c) and (d) show the results taking $(d_{\mathrm{Ru\text{-}Ar}}-d_0)=1$ and 2 Å, respectively, with $\Phi=5$ eV and $m^\star=0.2$ (solid lines) and 0.3 (dashed-dotted).

dependence $f(d_{\mathrm{Ru\text{-}Ar}},k_\parallel)$ is achieved. Thus, we have

$$\Gamma^{\mathrm{Ar}^\star 4s}(\epsilon_{4s}) \propto \int_{k_{min}(\epsilon_{4s})}^{k_{max}(\epsilon_{4s})} dk_\parallel k_\parallel |f(d_{\mathrm{Ru\text{-}Ar}},k_\parallel)\tilde{\phi}_{4s}(k_\parallel)|^2. \quad (32)$$

The factor $f(d_{\mathrm{Ru\text{-}Ar}},k_\parallel)$ in Eq. (31) reduces very efficiently the contribution of large values of $k_\parallel$ to the integral in Eq. (32) as the energy ϵ_{4s} moves downward. This explains the appearance of a maximum in Fig. 10(a). Figure 11 shows the results of Eq. (32) using several reasonable parameters for the Ar/Ru(0001) system. There is a clear qualitative agreement with the full calculation.

We now explore the effect of the nearest Ar neighbors around a given photoexcited Ar* atom. As mentioned above, most of our calculations have been performed for a simplified model corresponding to an Ar coverage of one monolayer, higher than that suggested by the experimental results.[52] It is, therefore, of crucial importance to check that our results do not critically depend on the Ar coverage. Figure 12 compares the results obtained using a 2×2 lateral supercell containing either a $\mathrm{Ar}^\star\mathrm{Ar}_3$ layer or one Ar* atom [Ru(0001)-(2×2)-Ar*, see Fig. 5]. In the latter case, the Ar*-Ar* distance is twice that of the Ar*-Ar distance in the former case. There is a downward shift of the 4*s* resonance, which is relatively moderate ($\sim$0.5 eV) at the experimental Ru-Ar distances. Thus, one of the main effects of the Ar neighbors seems to be the confinement of the 4*s* state of the Ar* atom, therefore increasing its energy. As a consequence, for small Ru-Ar separations, the effect of the projected band gap at Γ is smaller and the width is larger than in the case of larger Ar coverages. However, both curves cross as $d_{\mathrm{Ru\text{-}Ar}}$ increases. This result can be easily explained taking into account the reduction of the interaction matrix elements as we move to lower energies [Eq. (31)]. As the binding energy increases, the Ru states decay faster into the vacuum, and their overlap with the 4*s* orbital of the Ar* atom at large enough distances gets smaller. This effect translates into a faster decay of the $\Gamma_{isol}^{\mathrm{Ar}^\star\,4s}$ for the more diluted system. The experimental coverage of Ar on Ru(0001) is in between the two situations plotted in Fig. 12.

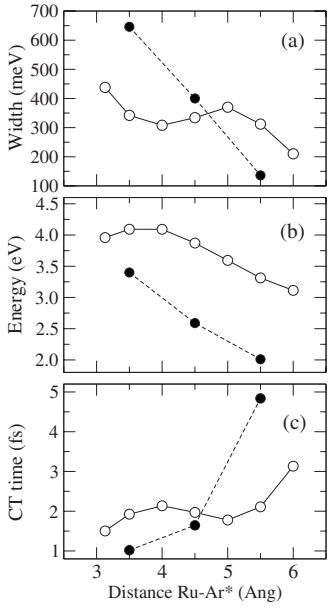

FIG. 12. Effect of the neighboring Ar atoms. Solid symbols correspond to a 2×2 supercell containing only one Ar* atom [Ru(0001)-(2×2)-Ar*, see also Fig. 5]. Open symbols stand for a $\mathrm{Ar}^\star\mathrm{Ar}_3$ layer (data also shown in Fig. 9). (a) $\Gamma_{isol}^{\mathrm{Ar}^\star\,4s}$ as a function of the distance between the argon adlayer and the ruthenium surface. (b) Position of the Ar* 4*s* resonance band minimum with respect to E_F. (c) Charge transfer time $\tau_{CT}=(\Gamma_{isol}^{\mathrm{Ar}^\star\,4s})^{-1}$.

C. Decay of an initial wave packet

To this point, we have extracted the charge transfer time of the 4*s* Ar* resonance from an analysis of the surface

Green's function. The width and the energy position of the different spectral features with an appreciable weight in the surface region are obtained from this analysis, and one of them is assigned to the 4*s* resonance. Alternatively, one could explore the time dynamics of a given initial wave packet. Such a calculation can be more appropriate to describe some experimental situations provided that a suitable wave packet can be constructed. This is not the case for the core hole-clock spectroscopy experiments available for the Ar/Ru(0001) system,[18,20] which have been performed with highly monochromatic light, but it might be the case for experiments performed using femtosecond or attosecond excitation pulses or, in general, wide-band excitation. In most cases, the wave packet will contain appreciable contributions from other resonances or continuum states besides the central resonance that one wants to study. Consequently, its dynamics will significantly depart from a simple exponential decay. This is clearly illustrated in Fig. 13(a) where the decay of the population of a wave packet initially localized in one Ar* atom in the $Ar^{\star}Ar_8$/Ru(0001) system is depicted as a function of $d_{\text{Ru-Ar}}$. Complex behavior appears in spite of the fact that the wave packets are constructed using a procedure that tries to ensure an optimum overlap with the true wave function of the 4*s* Ar* resonance. Our localized (Wannier-like) wave packets are constructed from a linear combination [Eq. (13)] of $\mathbf{k}_{\parallel}$ dependent extended (Bloch-like) wave packets as those shown in Figs. 7(c) and 7(d). These extended wave packets are the result of projecting the eigenfunctions of the 4*s* Ar* impurity band of the isolated argon layer onto the unoccupied states of the Ar/Ru(0001) system. The projection is performed in an energy window of 7 eV above E_F. The main peak of the 4*s* resonance appears well within this energy interval.

Only for the largest values of $d_{\text{Ru-Ar}}$ we recover in Fig. 13(a) a clear exponential decay. The interaction between the argon layer and the substrate is small in those cases and our wave packet, based on the 4*s* Ar* wavefunction of a free-standing layer, provides a good approximation for the resonance wave function. For smaller Ru-Ar distances, $|A^{cut}_{isol}(t)|^2$ contains at least three different contributions. Two of them are associated with the 4*s* resonance and represent, respectively, the components of the wave packet with $k_{\parallel}$ within the Ru projected band gap (notice that $k_{\parallel}$ refers here to a *k* vector of the lateral *supercell*, and the projected band gap is found for the surface *unit cell*), which decay with time constants of the order of several tens of femtoseconds, and those components outside the projected band gap with decay constants of the order of one to a few femtoseconds. These two contributions present a Lorentzian-like shape. The third contribution appears as a featureless background that extends to lower energies and takes into account the coupling with the continuum of Ru bulk states. This wide continuum contribution decays during the first few femtoseconds. The presence of the Fermi edge introduces a cutoff in this continuum background, which then oscillates with a well-defined frequency corresponding to the Fermi energy.

The curves in Fig. 13(a), at least for the smaller values of $d_{\text{Ru-Ar}}$, present a fast beating caused by the interference between the main Ar* 4*s* resonance and the continuum contribution. The frequency of this beating corresponds to the position of the 4*s* peak measured from the Fermi level.[70] This effect is quite robust with respect to changes of the electronic temperature defining the sharpness of the Fermi edge. As the temperature increases, the size of the oscillations decreases very slowly: for example, the shape of the time evolution curves is almost identical for values of β^{-1} as different as 1 eV and 25 meV. The beating only disappears for values of β^{-1} of several eV. An interesting question is whether this beating would be observable experimentally. A definite conclusion about this point is quite difficult to obtain for two main reasons. Firstly, the details of the initial electronic wave packet and thus of its time evolution depend on the way the excitation is created, e.g., the duration and spectral width of the excitation pulse, polarization of the excitation light, etc. These details, along with the coupling matrix elements between core and valence states, have to be taken into account in order to simulate a particular experiment. The second rea-

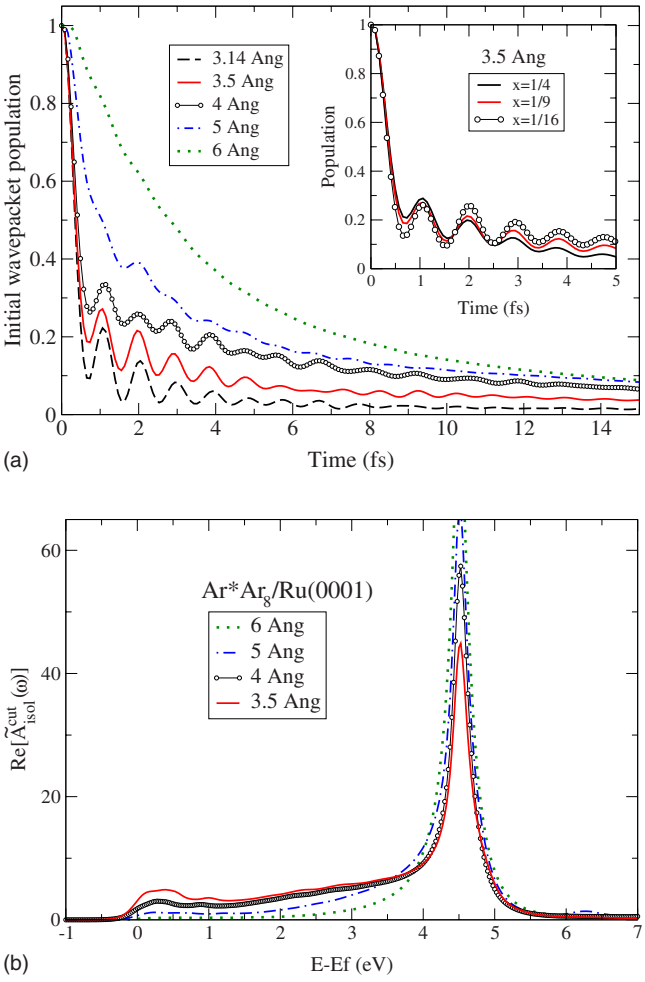

FIG. 13. (Color online) (a) Decay of the population ($|A^{cut}_{isol}(t)|^2$) of a wave packet initially localized in the Ar* of the $Ar^{\star}Ar_8$/Ru(0001) system as a function of the Ru-Ar distance. The inset shows the convergence of this time evolution as a function of the Ar* concentration for $d_{\text{Ru-Ar}}$=3.5 Å. (b) Real part of the Fourier transform of the survival amplitude [$\tilde{A}^{cut}_{isol}(\omega)$ in Eq. (22)] as a function of $d_{\text{Ru-Ar}}$.

son is the presence of inelastic processes, such as electron-electron scattering, which are not taken into account in our calculations. These processes are an important decoherence source once the electron penetrates into the solid and, therefore, likely to destroy many of the possible interference effects in the time evolution.

After the subtraction of the slowly decaying component (typically 10%–20% of the initial norm), for which the inelastic decay channels will be predominant, we can obtain the characteristic time constants τ_W for the population decay of our wave packet. To do this, we fit the decay of the maxima of the curves in Fig. 13(a) to an exponential. The values are 0.8, 1.0, 1.4, 2.2, and 4.0 fs as the $d_{\text{Ru-Ar}}$ increases. The fitting is rather poor for the smallest separation ($d_{\text{Ru-Ar}}$ =3.14 Å), pointing to the need of two different functional shapes to describe the behavior. However, the values of τ_W are in reasonable agreement with those given by the more careful approach presented in the previous section.

Figure 13(b) shows the real part of the Fourier transform of the survival amplitudes of our localized wave packets $[\tilde{A}_{isol}^{cut}(\omega)]$ as a function of $d_{\text{Ru-Ar}}$. They are clearly dominated by an asymmetric peak at the energy of the 4*s* resonance. The peak becomes narrower and more symmetric as $d_{\text{Ru-Ar}}$ is increased (notice though that these peaks are artificially widened due to our calculation outside the real axis, see Sec. II B). Fitting these peaks with a Lorentzian profile, we obtain the data listed in Table I under the label "Method 2." As $d_{\text{Ru-Ar}}$ decreases, the contribution from the continuum becomes larger as described above.

V. CONCLUSIONS

We have developed a scheme for the study of the resonant transfer of excited electrons from adsorbates to metal substrates. Our aim is to include a realistic description of the electronic structure of both the substrate and the adsorbate and the interaction between them. For this purpose, we use density-functional calculations of the adsorbate-substrate system using a slab geometry. The electronic Hamiltonian of the surface region is extracted, in a tight-binding form, from this calculation. These results are then combined with those of a bulk calculation of the substrate material in order to obtain the Hamiltonian of the semi-infinite system in which the electron evolves. Using this tight-binding-like Hamiltonian, we calculate the Green's function of the system with arbitrary energy resolution using recursive methods. In the present work, we have used the transfer matrix method. The Green's function is then projected onto a suitably chosen wave packet, and the widths and energies of the spectral features with appreciable weight in the surface area are obtained. These results are, in principle, independent of the wave packet utilized in the projection process. Using the projected Green's function, one can also calculate the dynamics of the population of the wave packet which, however, depends on the particular wave packet studied. This alternative can be quite useful to study very broad resonances[21] or to compare with experiments performed with excitation pulses of very short duration. However, one must analyze such results with care since the contributions from the continuum of bulk states or from other surface resonances, different from the studied one, can be significant. All our calculations are performed for periodic arrangements of adsorbates on the surface. We have discussed several ways to extrapolate to the limit of an isolated adsorbate using the appropriate averages of the $k_{\parallel}$ resolved results. Finally, since we want to focus on the case of core-excited adsorbates, we have discussed an approximate way to include the effect of the core hole in our calculation. In fact, we presented a scheme to approximate our initial state (before charge transfer to the substrate): an electron residing in a bound resonance associated with a core-excited adsorbate on the surface.

As an application, we have studied in detail the 4*s* bound resonance of a core-excited $Ar^*(2p_{3/2}^{-1}4s)$ atom in the Ar/Ru(0001) system, for which there are extensive experimental studies using core hole-clock spectroscopy. Our calculated charge transfer times range between 1.0 and 2.5 fs, in good agreement with the experimental value of 1.5 fs at resonance. To recover this value, it is instrumental to take into account the existence of a projected band gap in the electronic structure of the Ru(0001) substrate near Γ. We have carefully analyzed the dependence of the charge transfer rates on the Ru-Ar distance, the energy position of the resonance, and the distance between the $Ar^\star$ atom and its Ar neighbors. The projected band gap plays a fundamental role to understand all three behaviors. In particular, as already pointed out by Gauyacq and Borisov for the Ar/Cu(111) system,[68] it provides a simple explanation of the experimental observation that the charge transfer time can increase when the electrons are pumped to higher energies by the initial excitation. Our calculations reproduce this counterintuitive behavior quantitatively.

ACKNOWLEDGMENTS

D.S.-P. acknowledges useful discussions with R. Díez-Muiño, A. G. Borisov, and J.-P. Gauyacq. This work was supported by the Basque Departamento de Educación, Universidades e Investigación, the Basque Departamento de Industria, Comercio y Turismo, and the Diputación Foral de Gipuzkoa through the Etortek programme (grants NANOMATERIALES and NANOTRON), the University of the Basque Country UPV/EHU (Grant No. 9/UPV 00206.215-13639/2001), the Spanish Ministerio de Educación y Ciencia (Grant No. FIS2004-06490-C03-00 and FIS2007-66711-C02-02), and the EU Network of Excellence NANOQUANTA (Grant No. NMP4-CT-2004-500198). The work of D.M. was supported by the Fonds der Chemischen Industrie, Germany.

*sqbsapod@sc.ehu.es
†dietrich.menzel@ph.tum.de
‡wapetlap@sc.ehu.es

[1] See P. Feulner and D. Menzel in Ref. 2.
[2] *Laser Spectroscopy and Photochemistry on Metal Surfaces*, edited by H. Dai and W. H. (World Scientific, Singapore, 1995).
[3] W. Ho, Surf. Sci. **299/300**, 996 (1994).
[4] F. M. Zimmermann and W. Ho, Surf. Sci. Rep. **22**, 127 (1995).
[5] W. Ho, J. Phys. Chem. **100**, 13050 (1996).
[6] H. Petek and S. Ogawa, Prog. Surf. Sci. **56**, 239 (1997).
[7] M. Bauer, S. Pawlik, and M. Aeschlimann, Phys. Rev. B **55**, 10040 (1997).
[8] X.-Y. Zhu, Annu. Rev. Phys. Chem. **53**, 221 (2002).
[9] H. Petek and S. Ogawa, Annu. Rev. Phys. Chem. **53**, 507 (2002).
[10] P. M. Echenique, R. Berndt, E. V. Chulkov, T. H. Fauster, A. Goldmann, and U. Hofer, Surf. Sci. Rep. **52**, 219 (2004).
[11] P. S. Kirchmann, P. A. Loukakos, U. Bovensiepen, and M. Wolf, New J. Phys. **7**, 113 (2005).
[12] E. V. Chulkov, A. G. Borisov, J. P. Gauyacq, D. Sánchez-Portal, V. M. Silkin, V. P. Zhulkov, and P. M. Echenique, Chem. Rev. (Washington, D.C.) **106**, 4160 (2006).
[13] E. Goulielmakis, V. S. Yakovlev, A. L. Cavalieri, M. Uiberacker, V. Pervak, A. Apolonski, R. Kienberger, U. Kleineberg, and F. Krausz, Science **317**, 769 (2007).
[14] P. A. Brühwiler, O. Karis, and N. Mårtensson, Rev. Mod. Phys. **74**, 703 (2002).
[15] C. Keller, M. Stichler, G. Comelli, F. Esch, F. Lizzit, D. Menzel, and W. Wurth, J. Electron Spectrosc. Relat. Phenom. **93**, 135 (1998).
[16] Z. W. Gortel and D. Menzel, Phys. Rev. B **64**, 115416 (2001).
[17] F. Gel'mukhanov and H. Agren, Phys. Rep. **312**, 91 (1999).
[18] C. Keller, M. Stichler, G. Comelli, F. Esch, S. Lizzit, D. Menzel, and W. Wurth, Phys. Rev. B **57**, 11951 (1998).
[19] D. Menzel and W. Wurth, in *18th International Conference on X-ray and Inner-Shell Processes*, Chicago, 1999, edited by R. W. Dunford, D. S. Gemmell, E. P. Kanter, B. Kräsing, S. H. Southworth, and L. Young (AIP, Melville, NY, 2000), p. 372.
[20] W. Wurth and D. Menzel, Chem. Phys. **251**, 141 (2000).
[21] A. Föhlisch, P. Feulner, F. Hennies, A. Fink, D. Menzel, D. Sánchez-Portal, P. M. Echenique, and W. Wurth, Nature (London) **476**, 373 (2005).
[22] A. Föhlisch *et al.*, Chem. Phys. **289**, 107 (2003).
[23] A. G. Borisov, A. K. Kazansky, and J.-P. Gauyacq, Phys. Rev. B **59**, 10935 (1999).
[24] U. Fano, Phys. Rev. **124**, 1866 (1961).
[25] F. E. Olsson, M. Persson, A. G. Borisov, J.-P. Gauyacq, J. Lagoute, and S. Fölsch, Phys. Rev. Lett. **93**, 206803 (2004).
[26] L. Limot, E. Pehlke, J. Kröger, and R. Berndt, Phys. Rev. Lett. **94**, 036805 (2005).
[27] K. Niedfeldt, E. A. Carter, and P. Nordlander, J. Chem. Phys. **121**, 3751 (2004).
[28] K. Niedfeldt, P. Nordlander, and E. A. Carter, Phys. Rev. B **74**, 115109 (2006).
[29] J. E. Inglesfield, J. Phys. C **14**, 3795 (1981).
[30] J. E. Inglesfield and G. A. Benesh, Phys. Rev. B **37**, 6682 (1988).
[31] J. E. Inglesfield, Comput. Phys. Commun. **137**, 89 (2001).
[32] H. Ishida, Phys. Rev. B **63**, 165409 (2001).
[33] G. Butti, S. Caravati, G. P. Brivio, M. I. Trioni, and H. Ishida, Phys. Rev. B **72**, 125402 (2005).
[34] D. Sánchez-Portal, P. Ordejón, E. Artacho, and J. M. Soler, Int. J. Quantum Chem. **65**, 453 (1997).
[35] J. M. Soler, E. Artacho, J. D. Gale, A. García, J. Junquera, and D. Sánchez-Portal, J. Phys.: Condens. Matter **14**, 2745 (2002).
[36] E. Artacho and L. Miláns del Bosch, Phys. Rev. A **43**, 5770 (1991).
[37] L. M. Falicov and F. Yndurain, J. Phys. C **8**, 147 (1975).
[38] E. J. Mele and J. D. Joannopoulos, Phys. Rev. B **17**, 1816 (1978).
[39] D. H. Lee and J. D. Joannopoulos, Phys. Rev. B **23**, 4997 (1981).
[40] M. P. López-Sancho, J. M. López-Sancho, and J. Rubio, J. Phys. F: Met. Phys. **14**, 1205 (1984).
[41] M. P. López-Sancho, J. M. López-Sancho, and J. Rubio, J. Phys. F: Met. Phys. **15**, 851 (1985).
[42] E. Artacho and F. Yndurain, Phys. Rev. B **44**, 6169 (1991).
[43] C. Corriol, V. M. Silkin, D. Sánchez-Portal, A. Arnau, E. V. Chulkov, P. M. Echenique, T. von Hofe, J. Kliewer, J. Kröger, and R. Berndt, Phys. Rev. Lett. **95**, 176802 (2005).
[44] R. S. Mulliken, J. Chem. Phys. **23**, 1841 (1955).
[45] N. W. Ashcroft and N. D. Mermin, *Solid State Physics* (Saunders, Philadelphia, 1976).
[46] In principle, this is not only an efficient but even an exact way to eliminate the spurious effect of δ. It is evident, however, that for large values of t, the growing exponential factor in Eq. (24) will cause problems related to numerical accuracy. In practice, this is observed only for values of t much larger that those studied here ($\geqslant$50 fs).
[47] D. Sánchez-Portal, P. Ordejón, and E. Canadell, Struct. Bonding (Berlin) **113**, 103 (2004).
[48] W. Kohn and L. J. Sham, Phys. Rev. **140**, A1133 (1965).
[49] J. Junquera, O. Paz, D. Sánchez-Portal, and E. Artacho, Phys. Rev. B **64**, 235111 (2001).
[50] The cutoff radii of the different orbitals are $r_{5s}=r_{5p}=7.7$, $r_{4d}=5.3$, and $r_{4f}=5.6$ bohr for Ru. For Ar, we have $r_{3s}=4.0$, $r_{3p}=4.9$, $r_{4s}=10.0$, $r_{4p}=10.0$, and, $r_{3d}=6.0$ bohr.
[51] Our calculated lattice parameter a and c/a ratio for the hcp structure of bulk Ru are 2.702 Å and 1.580, respectively, to be compared with the experimental values of 2.70 Å and 1.584 (Ref. 45).
[52] B. Narloch, Ph.D. thesis, Technische Universität Muenchen, 1996, p. 158; B. Narloch and D. Menzel (unpublished).
[53] N. D. Lang, Phys. Rev. Lett. **46**, 842 (1981).
[54] J. L. F. Da Silva, C. Stampfl, and M. Scheffler, Phys. Rev. Lett. **90**, 066104 (2003).
[55] D. Menzel, Surf. Rev. Lett. **6**, 835 (1999).
[56] B. Narloch and D. Menzel, Chem. Phys. Lett. **270**, 163 (1997).
[57] R. D. Diehl, T. Seyller, M. Caragiu, G. S. Leatherman, N. Ferralis, K. Pussi, P. Kaukasoina, and M. Lindroos, J. Phys.: Condens. Matter **16**, S2839 (2004).
[58] S. Huzinaga, Comput. Phys. Rep. **2**, 281 (1985).
[59] G. Kresse and J. Hafner, Phys. Rev. B **47**, R558 (1993).
[60] G. Kresse and J. Furthmuller, Phys. Rev. B **54**, 11169 (1996).
[61] P. J. Feibelman, Phys. Rev. B **72**, 113405 (2005).
[62] J. P. Perdew, K. Burke, and M. Ernzerhof, Phys. Rev. Lett. **77**, 3865 (1996).
[63] The calculated structural parameters of bulk Ru with VASP are $a=2.682$ Å (2.720 Å) and $c/a=1.578$ (1.578) with LDA (GGA).
[64] W. Frieß, Ph.D. thesis, Technische Universität Muenchen, 1995, p. 118; W. Frieß, H. Schlichting, and D. Menzel (unpublished).
[65] P. J. Feibelman, Phys. Rev. B **26**, 5347 (1982).
[66] A. G. Borisov, D. Sánchez-Portal, R. D. Muiño, and P. M. Echenique, Chem. Phys. Lett. **387**, 95 (2004).

[67] A. G. Borisov, J. P. Gauyacq, E. V. Chulkov, V. M. Silkin, and P. M. Echenique, Phys. Rev. B **65**, 235434 (2002).
[68] J. P. Gauyacq and A. G. Borisov, Phys. Rev. B **69**, 235408 (2004).
[69] A. G. Borisov, J.-P. Gauyacq, A. K. Kazansky, E. V. Chulkov, V. M. Silkin, and P. M. Echenique, Phys. Rev. Lett. **86**, 488 (2001).
[70] Here, the spurious effects associated with the dispersion of the $Ar^{\star}$ 4*s* band are eliminated using formula Eq. (21). Accordingly, the average value (~4.5 eV) has been used for the relative position of the Fermi level and the $Ar^{\star}$ 4*s* resonance band.